Arabian Journal of Geosciences (2022) 15:791
https://doi.org/10.1007/s12517-022-10046-0

ORIGINAL PAPER

Mineral chemistry aspects of radioactive mineralization associated with Zr-, Nb-, and REE-bearing minerals from felsic dikes at Abu Hawis, North Eastern Desert, Egypt

Ahmed E. Abdel Gawad[1]

Received: 10 December 2021 / Accepted: 1 April 2022 / Published online: 14 April 2022

Abstract
The exposed rocks in Abu Hawis area, North Eastern Desert (NED), Egypt, consist of tonalite-granodiorite and monzogranite, dissected by post-granite felsic (microgranite and rhyolite) and mafic (basaltic-andesite) dikes. The investigated radioactive minerals and Zr-, Nb-, and REE-bearing minerals were restricted to felsic dikes having E–W and NE–SW trends. Uraninite, uranothorite, and thorite occur as the main radioactive minerals in microgranite dikes, while thorite is represent in rhyolite dikes. Y_2O_3 and HREE are recorded in zircon crystals from rhyolite dikes whereas HREEs in zircon grains from microgranite dikes are below detection limit. Zircon crystals from microgranite dikes contain high values of HfO_2 with up to 9.08 wt % owing to the effect of hydrothermal activity. Columbite from microgranite dikes has Ta/(Ta + Nb) and Mn/(Mn + Fe) ratios ranging between 0.0052–0.0164 and 0.0549–0.7010, respectively, which point to manganocolumbite composition, except for two spots that show a ferrocolumbite composition. Fergusonite is recorded in microgranite dikes, with average values of Nb_2O_5, Y_2O_3, and $HREE_2O_3$ reaching 50.3, 22.93, and 17.68 wt%, respectively. Monazite is recorded in both microgranite and rhyolite dikes, with marked enrichment of ThO_2, which reaches up to 12.52 wt% in the first one, while the total $\Sigma LREE_2O_3$ reached up to 68.5 wt% in the latter. Parisite and chevkinite are confined to rhyolite dikes with clear enrichment in LREE with averages ranging between 53.53 and 43.75 wt% $\Sigma LREE_2O_3$, respectively.

Keywords Abu Hawis · Egypt · Felsic dikes · E–W and NE–SW trends · Radioactive minerals · Rare metal mineralization

Introduction

The Arabian-Nubian Shield (ANS) is composed of basement rocks of Precambrian age along the Red Sea two flanks, located in western Arabia and northeastern Africa (Johnson and Woldehaimanot 2003; Liégeois and Stern 2010). The ANS was evolved in three stages, as follows: (a) Intra-ocean ridge subduction and arc magmatism >750 Ma, (b) collisional events and terrane amalgamation (~750 Ma–<620 Ma), (c) tectonic escape and extension <620 Ma (Farahat et al. 2011; Fathy et al. 2018). It consists of a large orogenic belt that extends from western Arabia to East African Orogen (EAO) (Fig. 1a), through Saudi Arabia, Yemen, Oman, Jordan, Egypt, Sudan, Eritrea, Ethiopia, and Somalia, whereas the southern belt occupies Mozambique segment.

Rare metal granites (RMG) are those enriched in one or more mineralization of the elements Zr, Nb, Ta, Rb, Cs, W, Sn, Li, F, Be, U, Th, REEs, and Y. RMG can be attributed either to magmatic and/or metasomatic processes (Abdalla et al. 1998; Gaafar et al. 2014; Dessouky et al. 2020; Ali et al. 2021; Abdel Gawad 2021). RMG intrusion occurred between 530 and 620 Ma during post-orogenic magmatism in the Egyptian Nubian Shield (Abdel Karim and Sos 2000; Moussa et al. 2008; Eliwa et al. 2014; Ali 2015; Skublov et al. 2021; Abdel Gawad et al. 2021a). However, rare metal mineralizations are mainly restricted to granites, pegmatites, acidic volcanics, and mylonite rocks as well as quartz and jasper veins widely distributed in the Eastern Desert of Egypt (Fig. 1b) (Saleh 2007; Raslan et al. 2010; Abdel Wahed et al. 2012; Dawoud et al. 2018; Heikal et al. 2001; 2019; Fawzy et al. 2020; Ghoneim et al. 2020; Surour and Omar 2020; Dessouky et al. 2020; Abdel Gawad et al.

Responsible Editor: Domenico M. Doronzo

✉ Ahmed E. Abdel Gawad
ahm.elsay@hotmail.com; gawadnma@gmail.com

[1] Nuclear Materials Authority, P.O. Box 530, El-Maadi, Cairo, Egypt

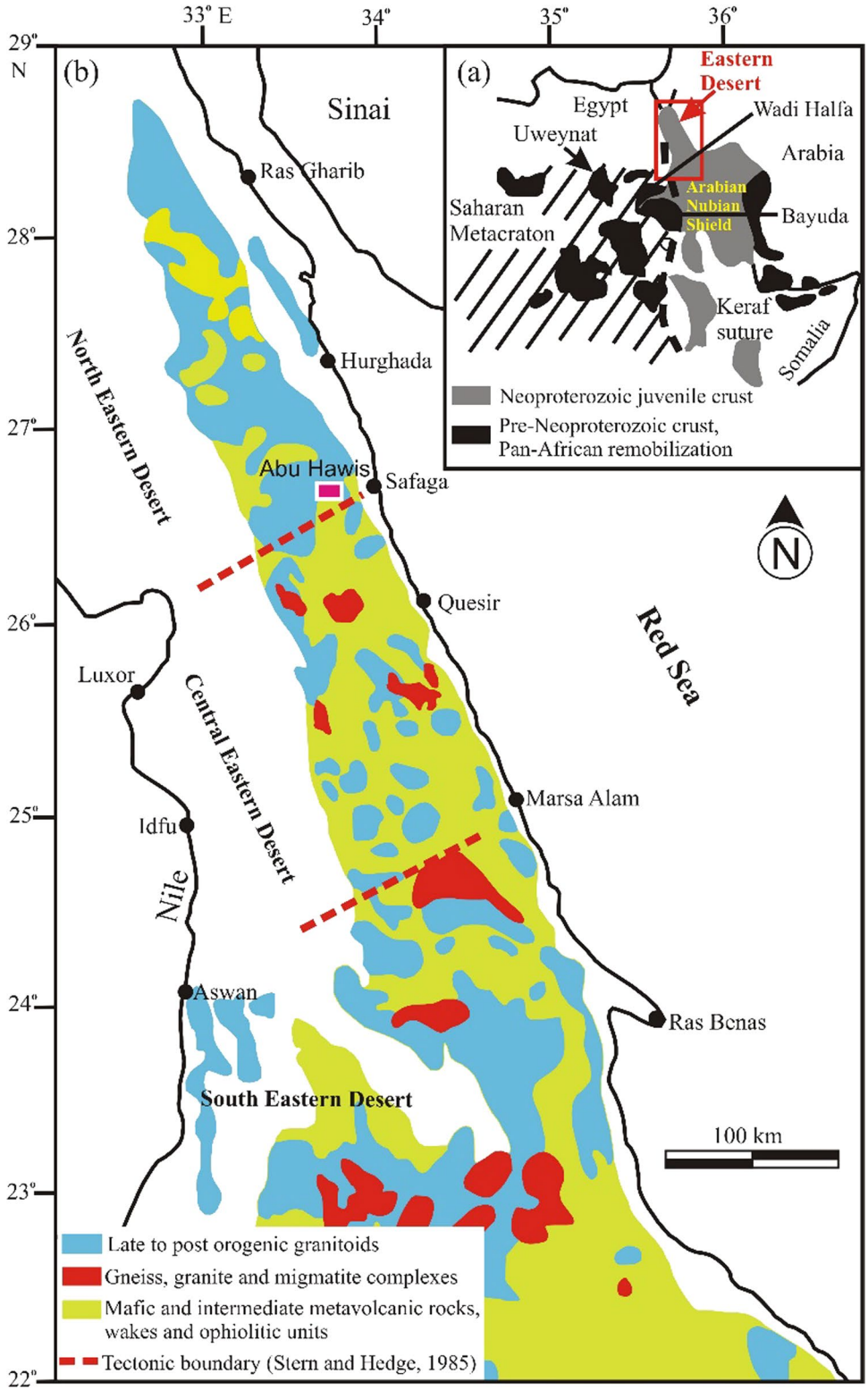

Fig. 1 **a** Geologic map of the Arabian Nubian Sheild (ANS); **b** geologic map of the basement rocks of Neoproterozoic age, Eastern Desert (ED), Egypt (Liégeois and Stern 2010)

2021b, c; Mahdy 2021; Surour 2021; Abdellah et al. 2021; Abdel Gawad et al. 2022; Surour and Omar 2022).

The need of rare metals has amplified intensely in the last few decades. Many of rare metals represent strategic economies, which are essential in the high technology, electronics, automobile industries, and renewable energy applications (Bourzac 2001; Eggert et al. 2010; Hoatson et al. 2011; Linnen et al. 2012).

Rare earth elements (REE) are considered as critical and vital material to future development. They are having a great importance, such as cell phones, computer memories, DVDs, rechargeable batteries, cerium oxide used for polishing gemstones such as granite and marble as well as glass, medical devices, high-efficiency motors in hybrid electric vehicles, catalytic converters, metallurgy, FeB magnets, wind power turbines, catalysts, and metal alloys as well as high demand for green energy and military defense systems (German and Elderfield 1990; Mariano and Mariano 2012; Gambogi 2013; Zepf 2013; Liu et al. 2013). Life demand is expected to increase dramatically over the next 10 years, without increase in the total REE reserves, thus highlighting the need to exploit for more REE deposits to be discovered (Hoatson et al. 2011; Jaireth et al. 2014). According to the high economical use of REEs, global request for REE will rise continuously, which will put great pressure on the current REE supply chain.

Several studies were carried out on Abu Hawis area (NED), Egypt (Ahmed and Moharem 2002; Al-Boghdady et al. 2005; Ali 2007; El-Bialy and Omar 2015; Dawoud et al. 2017). This paper presents in terms of novel data and interpretations about the mineralization especially U-, Th-, Zr-, Nb-, and REE-bearing minerals from the studied felsite dikes at Abu Hawis. To achieve this goal, micro-chemical analyses of these mineralization were first carried out in order to obtain informative data about radioactive minerals as well as Zr-, Nb-, and REE-bearing minerals.

Geologic setting

Field evidence shows that the exposed rock types are represented by tonalite-granodiorite, and monzogranite, which are cut by post-granite dikes and quartz veins (Figs. 2 and 3a–e).

The exposed rocks of Abu Hawis area are mostly composed of tonalite-granodiorite that have a huge batholith extending along the border of Qena–Safaga Road. They are medium- to coarse-grained rocks, form low relief, and vary from gray to whitish-gray colors. The pluton outcrops of these granitoids show marked intensive fracturing, jointing, exfoliation, and oval-like shapes, owing to the effect of weathering processes (Fig. 3f). They are strongly foliated and metamorphosed and occur as gneissose tonalite-granodiorite. Meanwhile, the other parts of tonalite-granodiorite occur as massive rocks. They are presented as small-sized plutons, without any deformed signatures. They are composed of quartz, plagioclase, K-feldspars, biotite, and hornblende.

The monzogranite pluton possesses circular to elliptical outlines and intrudes into tonalite-granodiorite of the studied area (Fig. 3f). It is frequently forming hard massive rocks,

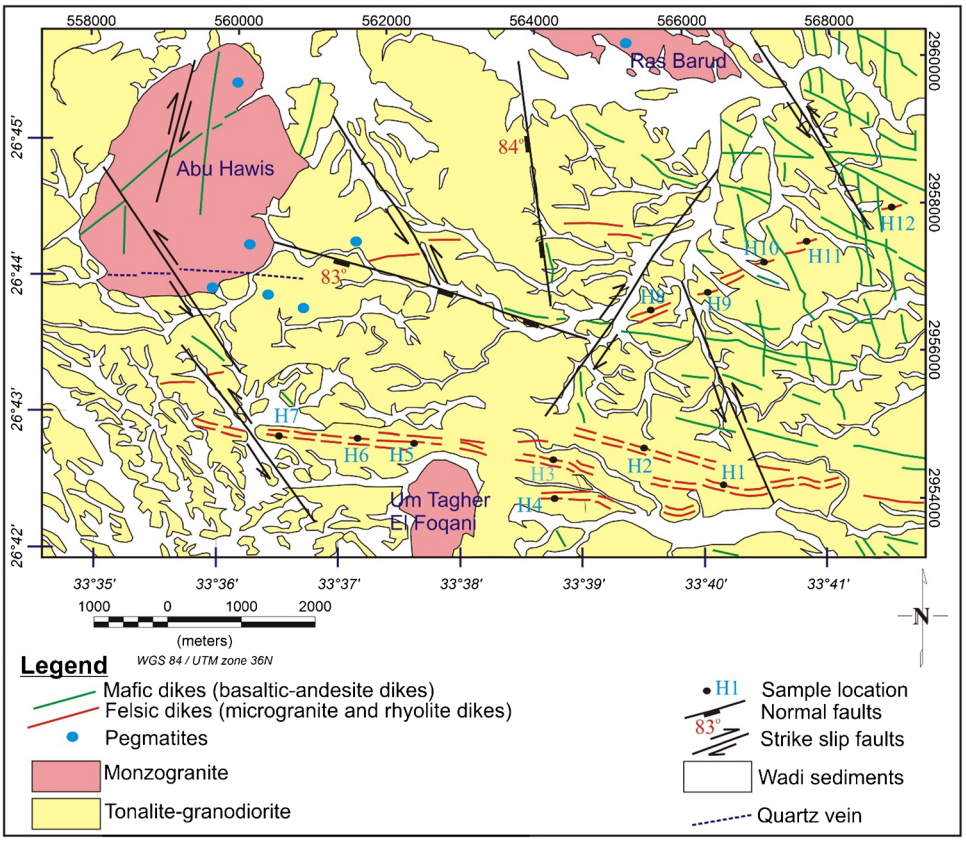

Fig. 2 Geologic map of Abu Hawis area, North Eastern Desert, Egypt (Ali 2007; El-Bialy and Omar 2015; Dawoud et al. 2017)

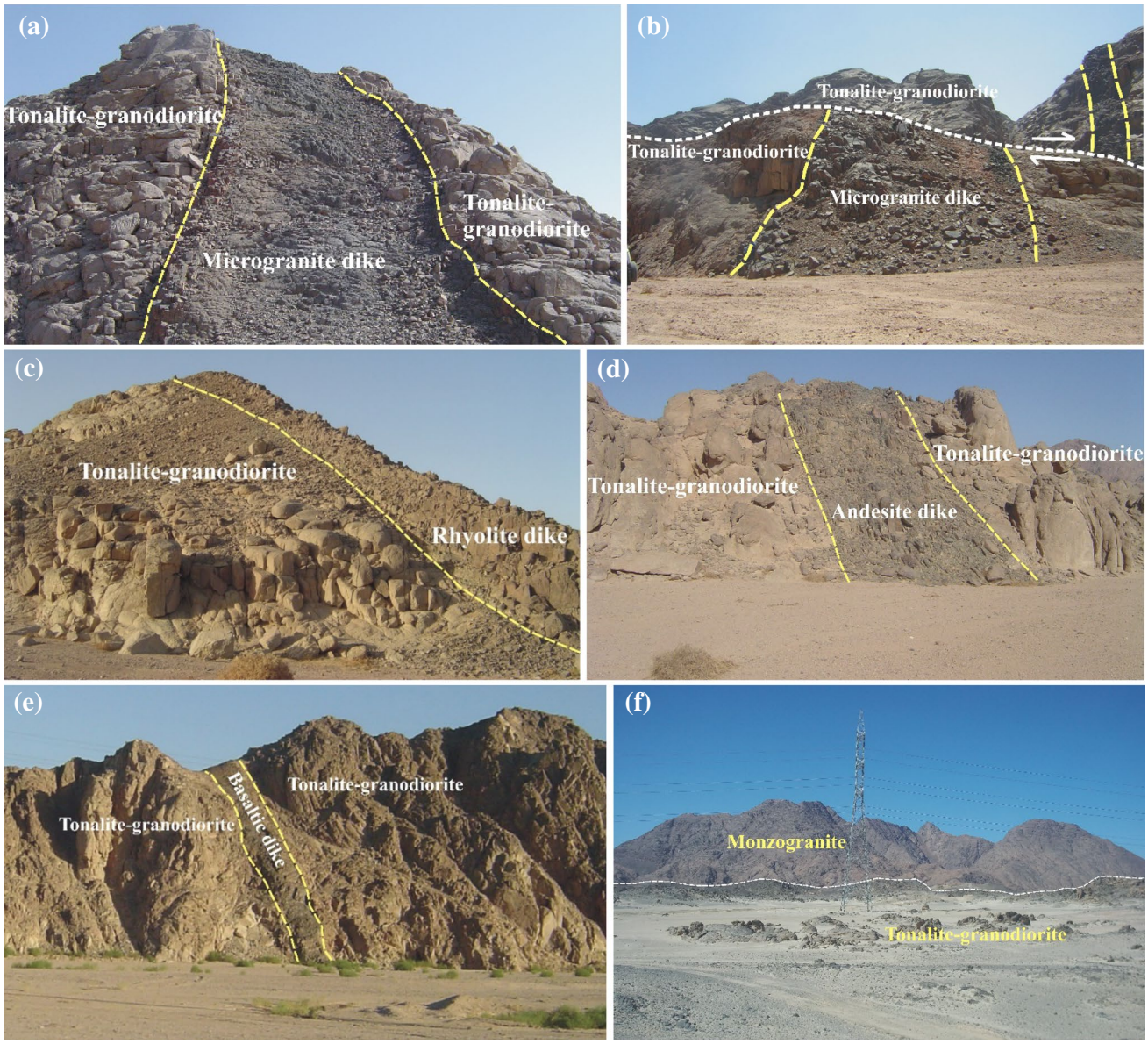

Fig. 3 **a** Microgranite dikes having E–W trend cross cut tonalite-granodiorite; **b** NE–SW strike-slip fault (right lateral) cross cut E–W microgranite dikes; **c** rhyolite dikes having NE–SW cross cut tonalite-granodiorite; **d** andesite dikes having NW–SE trend cross cut tonalite-granodiorite; **e** basaltic dikes having N–S trend cross cut tonalite-granodiorite; **f** tonalite-granodiorite rocks were intruded by the monzogranite (oval shape) with sharp intrusive contacts

high relief, pink to reddish brown in color, and medium- to coarse-grained. It is mainly composed of K-feldspar, quartz, plagioclase, muscovite, and biotite. Granitoids were dissected by basaltic-andesite dikes and quartz veins, striking in E–W, NW–SE, NE–SW, and N–S directions (Figs. 2 and 3d, e).

Pegmatites occur as pockets and/or dike-like forms. They are very coarse-grained, red, buff to reddish brown in color, and essentially composed of K-feldspar, quartz, plagioclase, biotite, and muscovite. They occur in the latest magmatic stages in Abu Hawis monzogranite and/or along the contacts between tonalite-granodiorite and monzogranite. Some exposures of these rocks are affected by hematitization and considered as good sources of strategic rare metal mineralization.

The most significant U mineralization occupies about 5 to 10 m width and 500 m length, subvertical, and highly altered basic dikes, striking in the NE–SW direction along the main shear zone of Abu Hawis plutons. Argillization, hematitization, and silicification are the main alterations affecting the sheared basic dikes. Relatively, high radioactive anomalies recorded in the main shear zone reached

about 80 ppm for eU and about 45 ppm for eTh, with an eU/eTh ratio reaching about 1.75 (Ammar et al. 2007).

Felsite dikes are cut through the tonalite-granodiorite. They range between 1 and 6 m width and are buff, pale pink to reddish brown color, are mostly fine-grained textures, and dominated by microgranite and rhyolite dikes. These dikes are mainly composed of quartz, K-feldspars, and plagioclase with mica as well as iron oxides. They are striking in the E–W and NE–SW directions with steeply dipping or nearly vertical (Fig. 3a–c). These dikes were jointed and fractured, highly altered, and affected by hematitization in addition to dendritic manganese oxides.

Materials and analytical methods

Twelve samples were selected and prepared in order to identify the petrographic characteristics of felsite dikes. Thin polished sections and slaps were prepared for microchemical analyses in order to investigate the rare metal mineralization especially in microgranite and rhyolite dikes. Mineral chemistry was obtained using an electron microprobe equipped with CAMECA SX 100, using five automated wavelength-dispersive spectrometers (WDS) and an energy-dispersive spectrometer (EDS). All performed analyses of minerals were made using the following conditions: the diameter of the electron beam on the specimen surface is under 1 µm, an acceleration voltage 15 kV, beam current 15 nA, counting time 10 s for peak, and 5 s for background. The standards used for calibration include natural standards such as albite for Al (Kα), orthoclase for Si (Kα), wollastonite for Ca (Kα), hematite for Fe (Kα), olivine for Mg (Kα), and monazite for Yb (Lα), whereas the synthetic compounds UO_2, ThO_2, ZrO_2, HfO_2, $PbCrO_4$, YPO_4, $LaPO_4$, $CePO_4$, $PrPO_4$, $NdPO_4$, $SmPO_4$, $EuRu_2Ge_2$, GdTiGe, $TbPO_4$, $DyRu_2Ge_2$, HoP_5O_4, $ErNi_2Si_2$, $TmPO_4$, $YbPO_4$, and $LuPO_4$ are used as standards for U (Mβ), Th (Mα), Zr (Lα), Hf (Mα), Pb (Mα), Y (Lα), La (Lα), Ce (Lα), Pr(Lß), Nd (Lα), Sm (Lα), Eu (Lα), Gd (Lα), Tb (Lα), Dy (Lα), Ho (Lβ), Er (Lα), Tm (Lα), Yb (Lα), and Lu (Lα) respectively. Pure metals of Nb and Ta were used for Nb–Ta-bearing minerals.

For an argillic sample, heavy liquids separation technique using bromoform of specific gravity 2.85 gm/cm^3 was used to concentrate the clay minerals. The clay minerals were picked under a binocular microscope to obtain pure mineral samples for X-ray diffraction (XRD) investigation. The X-ray diffraction (XRD) technique was used to identify the clay mineral sample using a PHILIPS PW 3710/31 diffractometer. These analyses were carried out in the laboratories of the Nuclear Materials Authority (NMA) of Egypt.

Results

Petrography of felsic dikes

Microgranite

Microscopically, microgranite shows equigranular texture and is composed mainly of K-feldspar, quartz, plagioclase, and muscovite (Fig. 4a). Zircon, pyrite, galena, sphalerite, and iron oxides are the most common accessory minerals, while sericite and kaolinite are the main alteration products. K-feldspar consists of microcline- and orthoclase microperthites. Microcline microperthite occurs as subhedral to euhedral crystals showing cross-hatched twinning (Fig. 4a). Orthoclase microperthite occurs as anhedral to subhedral crystals having simple twinning. Quartz occurs as interstitial grains between feldspar crystals as anhedral to subhedral crystals and fine grained. Plagioclase occurs as euhedral to subhedral tabular crystals. It exhibits simple and lamellar twinning (Fig. 4a, d). Muscovite occurs as anhedral crystals, corroded peripheries, and encloses opaques. Zircon crystals are coated by iron oxides, and occur as prismatic crystals enclosed in quartz and feldspars (Fig. 4b–d). Microgranite affected by hydrothermal alterations include kaolinization, chloritization, and hematitization (Fig. 4a–f).

Rhyolite

Rhyolite dikes are fine-grained and buff to reddish brown color and composed mainly of K-feldspars, quartz, and muscovite embedded in fine groundmass, showing porphyritic and spherulitic textures (Fig. 4g–j). Accessories are zircon, iron oxides, and opaque minerals, whereas sericite and kaolinite occur as secondary minerals. K-feldspar occurs either as subhedral to anhedral phenocrysts of orthoclase or as fine-grained groundmass in the matrix. Kaoline and sericite are the common alteration products of K-feldspar. Quartz occurs as subrounded to subangular phenocrysts and shows undulose extinction. Muscovite occurs as anhedral crystals and encloses zircon and iron oxides (Fig. 4g, h). Both kaolinization and hematitization were affected rhyolite (Fig. 4h–j).

Mineral chemistry

Uraninite, thorite, uranothorite, zircon, columbite, fergusonite, monazite, and parisite as well as pyrite, galena, sphalerite, apatite, and fluorite are well investigated from Abu Hawis felsic dikes, by using an electron probe microanalyses (EPMA) technique, as shown on Figs. 5–9 and Tables 1–5.

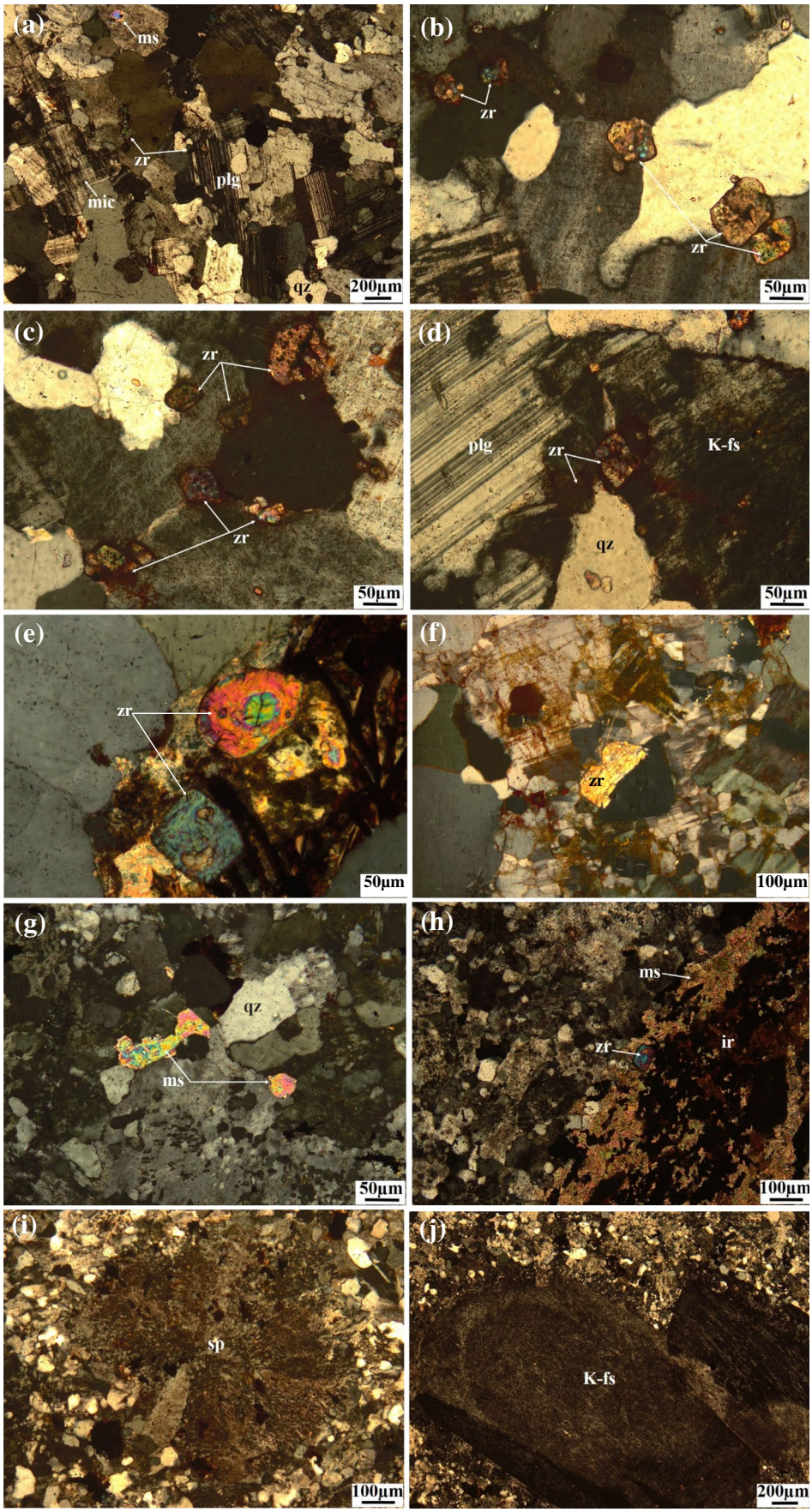

Fig. 4 Photomicrographs in felsic dikes of Abu Hawis area, North Eastern Desert, Egypt. **a** Microgranite is composed of plagioclase, microcline, quartz, and muscovite in addition to zircon and opaques, crossed nicols (C.N.); **b–d** zircon crystals are coated by iron oxides in microgranite (C.N.); **e** zircons surrounded by chlorite and iron oxides in microgranite (C.N.); **f** hematitization affected microgranite (C.N.); **g** muscovite in rhyolite (C.N.); **h** muscovite encloses zircon and iron oxides (hematitization) in rhyolite (C.N.); **i** spherulitic texture in rhyolite (C.N.); **j** K-feldspar shows porphyritic texture in rhyolite (C.N.). Abbreviations: plg, plagioclase; mic, microcline; K-fs, K-feldspar; ms, muscovite; zr, zircon; qz, quartz; ir, iron; sp, spherulitic

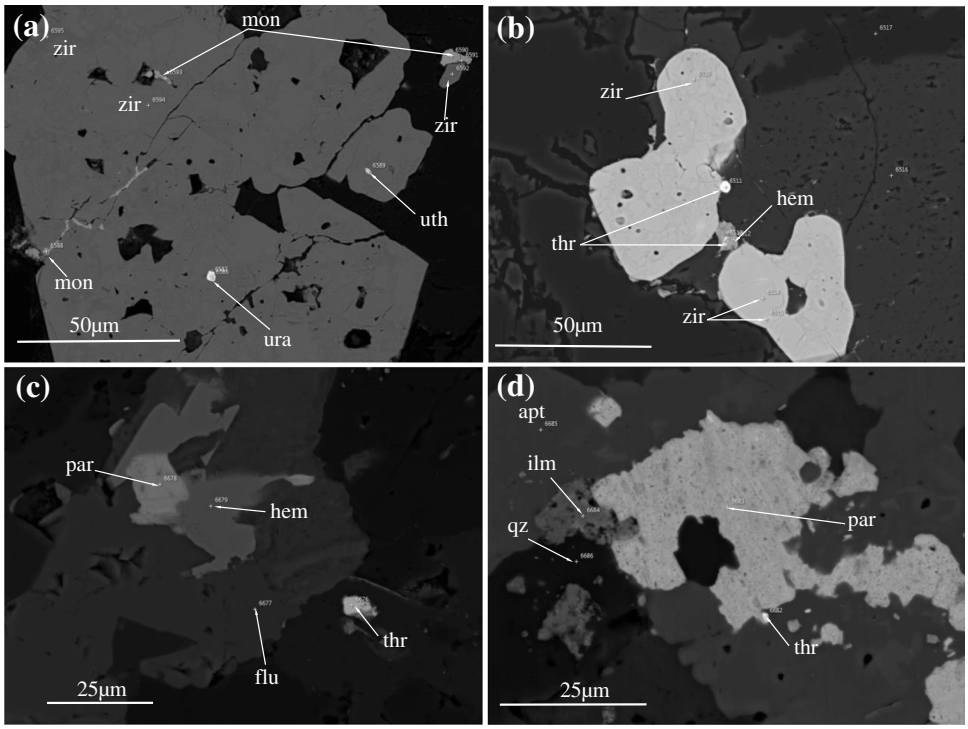

Fig. 5 SEM-BSE images of U- and Th-bearing minerals associated with other accessory minerals from felsic dikes, Abu Hawis area, North Eastern Desert, Egypt. **a** Micro-inclusions of uraninite, uranothorite, monazite, and opaques enclosed in large zircon crystals in microgranite; **b** fine thorite grains occurring along the peripheries of zircon in microgranite; **c** fine grained of thorite associated with parisite and fluorite in rhyolite; **d** thorite occurring along the peripheries of parasite in rhyolite. Abbreviations: ura, uraninite; uth, uranothorite; thr, thorite; Zir, zircon; mon, monazite; par, parisite; flu, fluorite; apt, apatite; qz, quartz; ilm, ilmenite; hem, hematite

Radioactive minerals

Uraninite is considered the main radioactive U-bearing mineral, while thorite and uranothorite are the main radioactive Th-bearing minerals in the studied microgranite and rhyolite dikes (Fig. 5a–d and Table 1).

Uraninite is recorded in peraluminous granites and their pegmatites as well as dolerite dikes (Gaafar et al. 2014; Ali et al. 2021; Ghoneim et al. 2021). It occurs as fine micro-inclusions that are enclosed in zircon crystals (Fig. 5a). Uraninite composed of UO_2 reached 69.1 and 69.57 wt%. PbO, Y_2O_3, and ThO_2 are present in uraninite and their contents reached up to 6.85, 8.2, and 4.02 wt%, respectively. Electron probe micro-analyzer (EPMA) data show that uraninite contains lower contents of SiO_2 and HREE, especially Dy_2O_3, Er_2O_3, and Yb_2O_3 (Table 1).

Thorite is a radioactive mineral. It is one of the most common Th-silicate minerals in felsic dikes of the area under investigation. It is enclosed as fine bright micro-inclusions in zircon crystals and shows intergrowth with zircon along its peripheries (Fig. 5b). It occurs as fine individual grains, subhedral to anhedral crystals (Fig. 5c). Other minute grains of thorite occur adjacent to parisite crystals (Fig. 5d). The chemical composition of thorite shows that the means of ThO_2 concentrations attain 57.89 and 61.69 wt% in both microgranite and rhyolite dikes, respectively. The means of SiO_2 contents reach 18.76 and 17.11 wt% in thorite from microgranite and rhyolite dikes, respectively. Thorite in microgranite dikes shows high mean values of UO_2, Y_2O_3, and ZrO_2 reaching 3.05, 3.39, and 0.51 wt%, when compared with thorite from rhyolite dikes. Dy_2O_3, Er_2O_3, and Yb_2O_3 were recorded as minor amounts in the studied thorite, but with higher mean contents in microgranite than those in rhyolite dikes (Table 1). CaO, P_2O_5, and Fe_2O_3 were recorded as minor constituents in the analyzed thorite (Table 1).

Uranothorite is a common Th-silicate mineral in microgranite dikes. It occurs as subrounded, subhedral grains, and micro-inclusions in zircon crystals (Fig. 5a). According to EPMA, the chemical composition of uranothorite reveals that ThO_2 concentration ranges between 49.89 and 51.17 wt%, UO_2 from 27.01 to 27.42 wt%, and SiO_2 from 17.25 to 18.04 wt% (Table 1). Small amounts of PbO, CaO, P_2O_5, Y_2O_3, ZrO_2, and Fe_2O_3 were detected, with means reaching 0.32, 0.89, 0.79, 0.33, 0.65, and 0.44 wt%, respectively.

Zircon

Zircon occurs as prismatic, subhedral to anhedral crystals, and varies from fine-grained to large crystals, reaching up to 200 µm in microgranite and rhyolite. It is associated with columbite, fergusonite, barite, rutile, ilmenite, hematite, and opaques (Fig. 6a–d). The presence of fine-grained zircon as micro-inclusion in large zircon crystals indicates the presence of two zircon generations, which are encountered in the studied microgranite dikes.

Table 1 Representative EPMA data (oxides, in wt%) of U and Th minerals from felsic dikes, Abu Hawis area, North Eastern Desert, Egypt

Min. in dike/oxid	Uraninite in microgranite		Thorite in microgranite				Aver	Thorite in rhyolite				Aver	Uranothorite in microgranite		
SiO_2	0.83	0.71	18.97	17.13	18.72	20.22	18.76	16.64	17.45	16.92	17.43	17.11	18.04	17.61	17.25
UO_2	69.1	69.57	4.32	5.33	1.28	1.28	3.05	1.27	1.23	1.08	1.22	1.20	27.42	27.21	27.01
ThO_2	3.19	4.02	56.72	57.38	58.93	58.51	57.89	61.67	61.32	62.59	61.18	61.69	50.17	49.95	49.89
PbO	6.85	6.83	n.d	n.d	n.d	n.d	n.d	n.d	n.d	n.d	n.d	n.d	0.35	0.32	0.29
CaO	n.d	n.d	1.41	0.99	1.24	1.45	1.27	0.98	1.51	1.19	1.57	1.31	1.03	0.87	0.76
P_2O_5	n.d	n.d	1.22	1.18	0.92	1.28	1.15	1.37	1.03	1.83	1.67	1.48	0.82	0.78	0.77
Y_2O_3	8.2	7.66	3.57	3.24	3.18	3.58	3.39	3.46	4.12	2.43	3.19	3.30	0.35	0.32	0.31
ZrO_2	n.d	n.d	0.25	0.58	0.97	0.24	0.51	0.63	0.26	0.21	0.22	0.33	0.71	0.67	0.58
Fe_2O_3	n.d	n.d	1.78	2.43	1.46	1.62	1.82	2.46	1.95	1.99	1.73	2.03	0.43	0.46	0.44
Dy_2O_3	2.72	2.78	0.62	0.58	0.65	0.63	0.62	0.57	0.45	0.53	0.61	0.54	n.d	n.d	n.d
Er_2O_3	3.24	3.08	0.55	0.45	0.44	0.51	0.49	0.49	0.47	0.48	0.51	0.49	n.d	n.d	n.d
Yb_2O_3	3.52	2.9	2.84	0.98	3.13	0.75	1.93	0.72	0.78	1.12	0.73	0.84	n.d	n.d	n.d
Total	97.65	97.55	92.25	90.27	90.92	90.07	90.88	90.26	90.57	90.37	90.06	90.32	99.32	98.19	97.30
Cation															
Si	0.04	0.03	0.99	0.94	1.00	1.04	0.99	0.91	0.95	0.92	0.94	0.93	0.96	0.95	0.94
U	0.66	0.67	0.05	0.06	0.02	0.01	0.04	0.02	0.01	0.01	0.01	0.01	0.32	0.33	0.33
Th	0.03	0.04	0.67	0.71	0.71	0.69	0.70	0.77	0.76	0.78	0.75	0.76	0.60	0.61	0.62
Pb	0.08	0.08											0.00	0.00	0.00
Ca			0.08	0.06	0.07	0.08	0.07	0.06	0.09	0.07	0.09	0.08	0.06	0.05	0.04
P			0.05	0.05	0.04	0.06	0.05	0.06	0.05	0.08	0.08	0.07	0.04	0.04	0.04
Y	0.19	0.18	0.10	0.09	0.09	0.10	0.10	0.10	0.12	0.07	0.09	0.10	0.01	0.01	0.01
Zr			0.01	0.02	0.03	0.01	0.01	0.02	0.01	0.01	0.01	0.01	0.02	0.02	0.02
Fe			0.07	0.10	0.06	0.06	0.07	0.10	0.08	0.08	0.07	0.08	0.02	0.02	0.02
Dy	0.04	0.04	0.01	0.01	0.01	0.01	0.01	0.01	0.01	0.01	0.01	0.01			
Er	0.044	0.042	0.01	0.01	0.01	0.01	0.01	0.01	0.01	0.01	0.01	0.01			
Yb	0.05	0.04	0.05	0.02	0.05	0.01	0.03	0.01	0.01	0.02	0.01	0.01			
∑cations	1.12	1.11	2.08	2.07	2.08	2.07	2.08	2.07	2.09	2.06	2.07	2.07	2.03	2.03	2.02

Min., mineral; *oxid.*, oxides; *Aver.*, average

Calculated chemical formulae are based on 2 oxygen atoms (apfu) for uraninite

Calculations are based on 4 oxygen atoms per formula unit (apfu) for thorite and uranothorite

n.d., not determined

According to EPMA (Table 2), zircon crystals from microgranite dikes are composed of ZrO_2 that ranges from 56.06 to 62.76 wt% and a mean reaching 60.09 wt%, SiO_2 from 30.76 to 34.29 wt% and a mean reaching 32.19 wt%, and HfO_2 from 1.03 to 9.08 wt% and a mean reaching 3.81 wt%. HfO_2 shows higher concentrations in the analyzed zircon crystals, reaching to 7.41, 9.08, and 6.12 wt% (Table 2). ThO_2 and UO_2 were recorded in zircon crystals and show low concentrations reaching up to 2.16 and 0.54 wt%, respectively. Only Yb_2O_3 from HREE is recorded with low contents. Minor amounts of CaO, Fe_2O_3, and Al_2O_3 were also recorded (Table 2).

On the other hand, EPMA data show that zircon crystals from rhyolite dikes are composed essentially of ZrO_2, ranging from 58.46 to 59.21 wt% and a mean reaching 58.72 wt%, SiO_2 from 29.73 to 30.29 wt% and a mean attaining 30.0 wt%, and HfO_2 from 0.98 to 3.09 wt% and a mean reaching 1.59 wt%. ThO_2 and UO_2 display low concentrations in the analyzed zircon crystals with mean values of 0.74 and 0.85 wt%, respectively. HREE (Dy_2O_3, Er_2O_3, and Yb_2O_3) and Y_2O_3 were recorded in the analyzed zircon crystals, with mean values reaching 0.54, 0.63, 1.06, and 4.03, respectively (Table 2). CaO and Fe_2O_3 were also recorded in zircon crystals as minor constituents.

Nb-rich minerals

Columbite occurs as anhedral to subhedral crystals, up to 100 µm in microgranite, commonly enclosed in plagioclase, K-feldspar, and quartz crystals. Other columbite crystals are dispersed as fine- to medium-grained crystals enclosed in fergusonite (Fig. 6c). Some crystals of

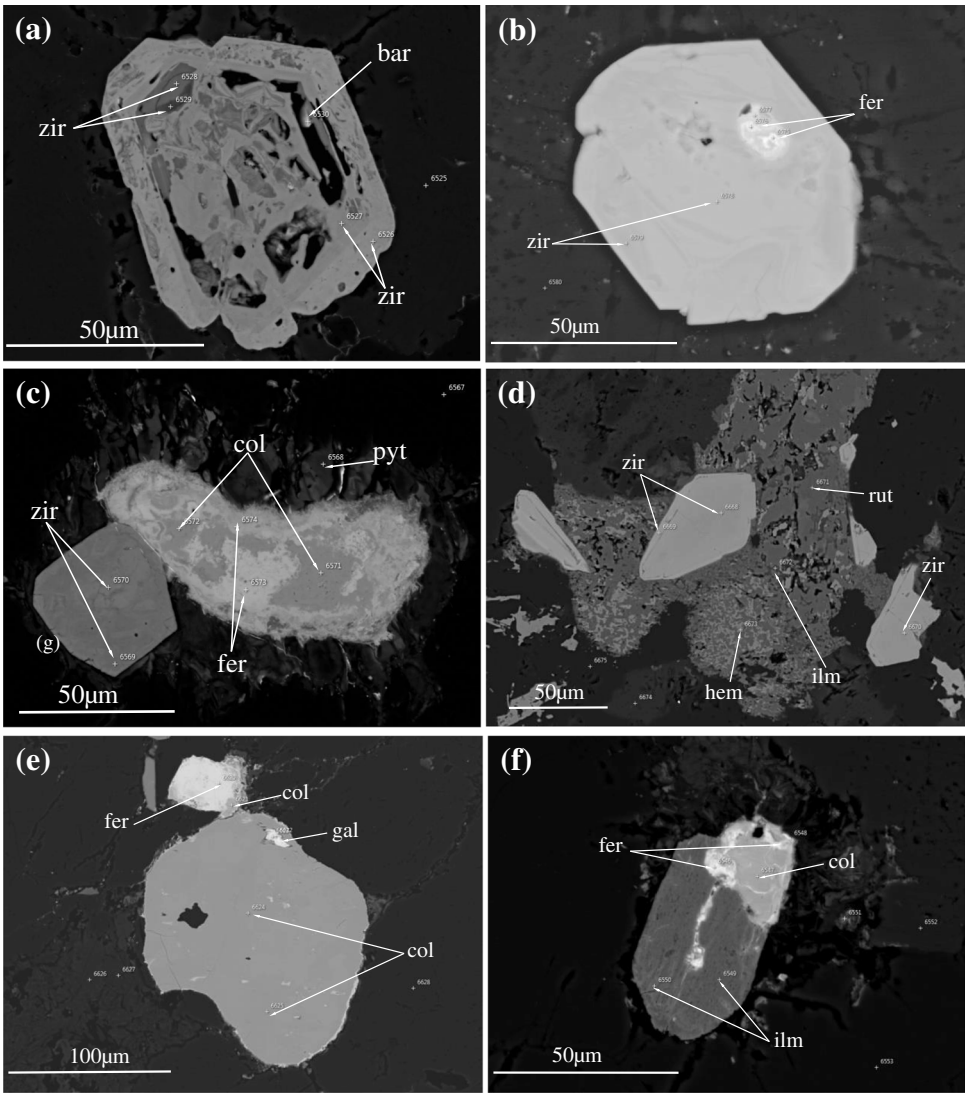

Fig. 6 SEM-BSE images of Zr- and Nb-bearing minerals, associated with other accessory minerals from felsic dikes, Abu Hawis area, North Eastern Desert, Egypt. **a** Faint zoning of zircon enclosing micro-inclusions of zircon, barite, and opaques in microgranite; **b** micro-inclusions of fergusonite enclosing zircon in microgranite; **c** fergusonite enclosing columbite, adjacent to zircon in microgranite; **d** zircon crystals associated with rutile, ilmenite, and hematite in rhyolite; **e** micro-inclusions of galena enclosed in a large crystal of columbite that is associated with fergusonite in microgranite; **f** columbite and fergusonite adjacent to the peripheries of ilmenite in microgranite. Abbreviations: zir, zircon; bar, barite; fer, fergusonite; col, columbite; pyt, pyrite; gal, galena; ilm, ilmenite; hem, hematite; rut, rutile

columbite enclose micro-inclusions of galena and opaque minerals (Fig. 6e). EPMA analyses reveal that the typical composition of manganocolumbite, according to the quadrilateral diagram of Černý and Ercit (1985), except two spots is ferrocolumbite composition (Fig. 7). EPMA data reveal that manganocolumbite is composed of Nb_2O_5, which ranges between 65.26 and 73.34 wt% with a mean value of 73.24 wt%. MnO shows high concentrations that reached 14.95 wt%, with marked lower contents in two spots 1.1 and 1.52 wt%. Meanwhile, Fe_2O_3 reached up to 18.11 wt%. Y_2O_3, Ta_2O_5, TiO_2, and CaO are represented in low concentrations, with means attaining 0.53, 1.48, 2.88, and 028, respectively. UO_2 and ThO_2 have quite low concentration in the analyzed samples, reaching up to 1.43 and 1.75 wt%, respectively.

Ta/(Ta + Nb) ratios of columbite range from 0.0052 to 0.0164, whereas Mn/(Mn + Fe) ratios show a marked wide range, from 0.0549 to 0.7010. These two ratios could indicate enrichment of manganese in the analyzed manganocolumbite composition except the two spots enriched in iron (Table 3 and Fig. 7).

Fergusonite occurs as subhedral to anhedral and fine-grained, while some crystals are strongly deformed and corroded along their peripheries. It is enclosed in zircon crystals as micro-inclusions and occurs along the peripheries of columbite as thin inclusions (Fig. 6b, f). Other fergusonite crystals poikilitically enclose columbite (Fig. 6c). EPMA analyses of fergusonite show that Nb_2O_5 ranges between 48.6 and 51.95 wt%, a mean of 50.3 wt%, and Y_2O_3 between 22.13 and 23.64 wt%, a mean of 22.93 wt%. It represents one of the main resources which carry heavy rare earth elements, where the total HRE_2O_3 (Gd_2O_3-Lu_2O_3) ranges between 16.2 and 19.08 wt%, a mean of 17.68 wt%. Ta_2O_5 and TiO_2 show low concentration, with means attaining 0.77 and 1.02 wt%, respectively. UO_2 and ThO_2 reached up to 3.82 and 2.94

Table 2 Representative EPMA data (oxides, in wt%) of zircon from felsic dikes, Abu Hawis area, North Eastern Desert, Egypt

Min. in dike/oxid	Zircon in microgranite							Aver	Zircon in rhyolite				Aver
SiO_2	31.27	31.02	32.97	30.76	31.41	33.64	34.29	32.19	30.24	29.73	30.29	29.75	30.00
ZrO_2	60.44	61.21	62.53	56.06	60.46	57.19	62.76	60.09	59.21	58.46	58.64	58.56	58.72
HfO_2	7.41	2.28	1.73	9.08	6.12	2.26	1.26	4.31	3.09	1.23	1.06	0.98	1.59
CaO	n.d	1.29	0.89	2.04	n.d	2.52	n.d	1.69	1.24	n.d	n.d	0.92	1.08
Fe_2O_3	n.d	0.72	0.77	0.63	0.47	1.32	0.86	0.80	1.12	1.54	0.86	1.44	1.24
Al_2O_3	n.d	0.86	0.34	n.d	0.38	0.61	n.d	0.55	n.d	n.d	n.d	n.d	n.d
ThO_2	0.34	2.16	0.33	0.24	0.41	1.10	0.35	0.70	1.19	0.49	0.54	0.75	0.74
UO_2	0.54	0.46	0.38	0.53	0.39	0.42	0.43	0.45	0.82	0.87	0.92	0.77	0.85
Y_2O_3	n.d	n.d	n.d	n.d	n.d	n.d	n.d	n.d	1.31	5.09	5.12	4.59	4.03
Dy_2O_3	n.d	n.d	n.d	n.d	n.d	n.d	n.d	n.d	0.45	0.59	0.62	0.48	0.54
Er_2O_3	n.d	n.d	n.d	n.d	n.d	n.d	n.d	n.d	0.31	0.75	0.77	0.67	0.63
Yb_2O_3	n.d	n.d	n.d	0.63	0.36	0.58	n.d	n.d	1.02	1.07	1.18	0.95	1.06
Total	100	100	99.94	99.97	100	99.64	99.95	99.93	100	99.82	100	99.86	99.92
Cation	Calculated chemical formulae are based on 4 oxygen atoms (apfu)												
Si	0.99	0.97	1.01	0.99	0.99	1.03	1.04	0.99	0.96	0.95	0.97	0.95	0.95
Zr	0.93	0.93	0.93	0.88	0.93	0.85	0.93	0.90	0.92	0.91	0.91	0.91	0.91
Hf	0.07	0.02	0.02	0.08	0.06	0.02	0.01	0.04	0.03	0.01	0.01	0.01	0.01
Ca	0.00	0.04	0.03	0.07	0.00	0.08	0.00	0.06	0.04	0.00	0.00	0.03	0.04
Fe	0.00	0.02	0.02	0.02	0.01	0.03	0.02	0.02	0.03	0.04	0.02	0.03	0.03
Al	0.00	0.03	0.01	0.00	0.01	0.02	0.00	0.02	0.00	0.00	0.00	0.00	0.00
Th	0.00	0.02	0.00	0.00	0.00	0.01	0.00	0.00	0.01	0.00	0.00	0.01	0.01
U	0.00	0.00	0.00	0.00	0.00	0.00	0.00	0.00	0.01	0.01	0.01	0.01	0.01
Y	0.00	0.00	0.00	0.00	0.00	0.00	0.00	0.00	0.02	0.09	0.09	0.08	0.07
Dy	0.00	0.00	0.00	0.00	0.00	0.00	0.00	0.00	0.00	0.01	0.01	0.00	0.01
Er	0.00	0.00	0.00	0.00	0.00	0.00	0.00	0.00	0.00	0.01	0.01	0.01	0.01
Yb	0.00	0.00	0.00	0.01	0.00	0.01	0.00	0.00	0.01	0.01	0.01	0.01	0.01
∑cations	2.00	2.03	2.02	2.04	2.01	2.06	2.00	2.04	2.04	2.04	2.03	2.05	2.05

Min, mineral; *oxid*, oxides; *Aver.*, average; *n.d.*, not determined

wt%, respectively. Minor amounts of CaO, MnO, Fe_2O_3, and SiO_2 were recorded (Table 3). The chemical formula of fergusonite is $A^{3+}B^{5+}O_4$. A-site is dominated by Y and REE, whereas B-site is occupied by Nb, Ta, and Ti. Other cations could occur in A-site. The calculated chemical formula of fergusonite is mentioned as follows:

$$(Y_{0.53}Gd_{0.01}Dy_{0.04}Ho_{0.01}Er_{0.06}Tm_{0.02}Yb_{0.08}Lu_{0.01}U_{0.02}Fe_{0.04}Ca_{0.04}Th_{0.02})$$
$$(Nb_{0.99}Ta_{0.01}Ti_{0.03})O4$$

REE minerals

A. Monazite-Ce is a common REE-phosphatic mineral. It is always present in the studied felsic dikes. It occurs as anhedral to subhedral, fine-grained, micro-veinlets, and is observed as micro-inclusions in zircon and parisite crystals (Figs. 5a and 8a, b). The chemical composition of monazite using EPMA is shown on Table 4. EPMA data of the analyzed monazite from the microgranite reveal that P_2O_5 ranges from 26.66 to 30.98 wt% and a mean reaching 29.35 wt%. The total REE oxides oscillate from 55.97 to 60.19 wt% and a mean reaching 58.38 wt%. Ce_2O_3 is often a common REE that varies from 28.76 to 31.95 wt% and a mean reaching 30.42 wt%, which designates monazite-Ce. The abundance of Ce_2O_3 is followed by Nd_2O_3, La_2O_3, Pr_2O_3, and Sm_2O_3, with a mean attaining values 11.19, 9.17, 4.35, and 2.05 wt%, respectively. Gd_2O_3 is the only heavy rare earth element, recorded in monazite, reaching up to 1.37 wt%. Monazite grains are enriched in ThO_2 concentrations ranging from 10.11 to 11.98 wt% and a mean reaching 11.29 wt%. SiO_2, CaO, and Fe_2O_3 occur in minor concentrations (Table 4).

On the other hand, EPMA data show that the chemical composition of monazite crystals from rhyolite is composed mainly of P_2O_5 that ranges from 28.48 to 29.32 wt% and a mean reaching 29.08 wt%. The total $\sum REE_2O_3$ content ranges from 67.82 to 68.50 wt% and a mean reaching 68.14

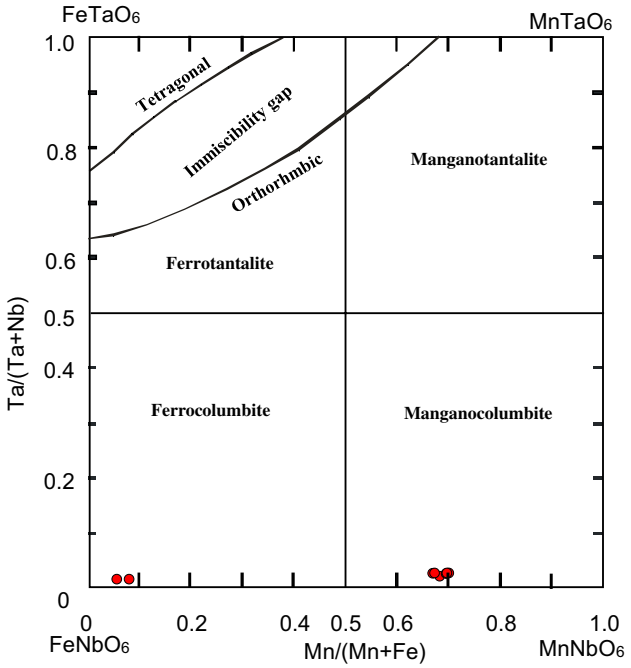

Fig. 7 Quadrilateral diagram according to Černý and Ercit (1985) illustrating the chemical composition of columbite-tantalite from the microgranite, Abu Hawis area, North Eastern Desert, Egypt

wt%. Ce_2O_3 is the most abundant REE element. It ranges from 32.24 to 33.06 wt% and a mean reaching 32.62 wt%, followed by La_2O_3 with a mean attaining 15.85 wt%, then Nd_2O_3 with a mean attaining of 14.17 wt%, Pr_2O_3 with a mean reaching 3.12 wt%, and Sm_2O_3 with a mean attaining 1.60 wt%. Gd_2O_3 is the only recorded HREE in the analyzed monazite, with a mean reaching 0.79 wt%. ThO_2 shows low concentration in the monazite grains, with a mean of 1.53 wt%. SiO_2, CaO, and Fe_2O_3 are present at lesser concentrations, with mean values of 0.22, 0.31, and 0.35 wt%, respectively (Table 4).

The chemical formula of monazite could be expressed as follows: (Ce, La, Nd, Sm, Th)PO_4. The fundamental chemical formulae of average monazite grains in the microgranite and the rhyolite are as follows: $(Ce_{0.44}Nd_{0.16}La_{0.14}Pr_{0.06}Sm_{0.03}Gd_{0.02}Th_{0.10})(P_{0.99}Si_{0.01})O_4$ and $(Ce_{0.47}Nd_{0.20}La_{0.23}Pr_{0.05}Sm_{0.02}Gd_{0.01}Th_{0.01})(P_{0.98}Si_{0.01})O_4$, respectively. It is clear that the analyzed monazite shows a predominance of Ce, up to (0.47 apfu), over the other REEs designating monazite-Ce.

B. Parisite-(Ce) is always present only in rhyolite. It is a calcium REE-fluorocarbonate mineral and occurs as anhedral to subhedral large grains up to 100 µm (Figs. 5d and 8b, c). Some corroded parisite crystals are in parallel intergrowth with monazite. Parisite occurs in association with fluorite, hematite, and thorite while the latter mineral, in some cases, occurs along the peripheries of parisite crystals (Fig. 5d). From the EMP analyses (Table 5), parisite shows a strong enrichment in LREE. It is essentially composed of CaO that ranges from 12.84 to 14.87 wt%, with a mean of 13.8 wt%. The total $\sum REE_2O_3$ ($La_2O_3 + Ce_2O_3 + Pr_2O_3 + Nd_2O_3 + Sm_2O_3 + Gd_2O_3$) concentrations range from 52.28 to 55.21 wt%, with a mean of 53.53 wt%. Ce_2O_3 is considered the most predominant LREE in parisite. It ranges from 22.09 to 23.91 wt% with a mean of 22.99 wt%. La_2O_3 and Nd_2O_3 show high concentrations in parisite, with mean values of 14 and 11.71 wt%, respectively, then Pr_2O_3 followed by Sm_2O_3 and then Gd_2O_3, in ascending magnitudes (Table 5). ThO_2 and SiO_2 are present in minor amounts, with mean values of 0.64 and 0.12 wt%, respectively. The empirical chemical formula of average parisite grains in rhyolite is as follows: $Ca_{1.02}(Ce_{0.58}La_{0.36}Nd_{0.29}Pr_{0.08}Sm_{0.04}Gd_{0.01})_2(CO_3)_3F_{1.84}$.

C. Chevkinite-(Ce) occurs as fine-grained crystals, up to 5 µm in length (Fig. 8d), subrounded to subhedral, and enclosed in quartz. It is recorded only in the rhyolite of the study area and has a limited abundance. It is a titanosilicate REE mineral. As a result of EPMA data, chevkinite crystals from the rhyolite are mainly composed of SiO_2 TiO_2, and Fe_2O_3 that reached up to 19.97, 20.35, and 13.11 wt%, respectively (Table 5). The analyzed EPMA data indicate that chevkinite shows considerably higher $\sum LREE_2O_3$ (La_2O_3–Sm_2O_3) concentrations, reaching up to 44.21 wt% (Table 5). Chevkinite is enriched in LREE and Ce_2O_3 is the main predominant REE that reaches 21.52 and 21.85 wt% corresponding to chevkinite-(Ce) in chemical composition. La_2O_3 shows high concentrations reaching to 11.38 and 11.56 wt% and Nd_2O_3 7.87 and 8.24 wt%, while Pr_2O_3 and Sm_2O_3 show low concentrations in the analyzed samples (Table 5). ThO_2 and UO_2 are present in minor amounts, up to 2.11 and 0.22 wt%, respectively. CaO and P_2O_5 are recorded also in minor amounts, up to 1.65 and 0.09 wt%, respectively and/or not recorded.

The chemical composition of chevkinite has the formula $A_4BC_2D_2(Si_2O_7)_2O_8$, where the cations are represented in each site as follows: A = REE^{3+}, Ca^{2+}; B = Fe^{2+}; C = Fe^{2+}, Fe^{3+}, Ti^{4+}, Al^{3+}; D, Ti^{4+} according to Macdonald et al. (2012) and Bagiński et al. (2015).

Other accessory minerals

Sulfide minerals including pyrite, galena, and sphalerite are recorded in the microgranite, whereas fluorite and fluorapatite are presented in the rhyolite.

Pyrite occurs as fine-grained, anhedral grains associated with fergusonite, columbite, and zircon in the microgranite (Fig. 6c). Other pyrite grains, associated with galena, are disseminated throughout plagioclase (Fig. 9a). EPMA data show that the chemical composition of pyrite is Fe reaching 47.03 wt% and S attaining 52.74 wt%.

Table 3 Representative EPMA data (oxides, in wt%) of Nb-rich minerals from microgranite dikes, Abu Hawis area, North Eastern Desert, Egypt

Min./oxid	Columbite								Fergusonite				
Y_2O_3	0.84	0.42	0.45	0.43	0.98	0.62	n.d	n.d	22.16	23.15	22.13	23.58	23.64
Nb_2O_5	72.07	73.03	74.68	73.53	71.31	71.8	74.57	74.93	48.6	51.95	50.77	51.19	48.97
Ta_2O_5	1.89	1.62	1.64	1.67	1.81	1.79	0.73	0.72	0.78	0.81	0.75	0.79	0.74
Gd_2O_3	n.d	n.d	n.d	n.d	n.d	n.d	n.d	n.d	1.15	0.63	0.64	0.62	0.58
Dy_2O_3	n.d	n.d	n.d	n.d	n.d	n.d	n.d	n.d	3.24	2.64	3.27	2.43	2.75
Ho_2O_3	n.d	n.d	n.d	n.d	n.d	n.d	n.d	n.d	0.89	1.02	1.1	0.73	1.13
Er_2O_3	n.d	n.d	n.d	n.d	n.d	n.d	n.d	n.d	4.37	4.44	4.86	4.38	5.22
Tm_2O_3	n.d	n.d	n.d	n.d	n.d	n.d	n.d	n.d	0.75	1.53	0.78	1.02	1.93
Yb_2O_3	n.d	n.d	n.d	n.d	n.d	n.d	n.d	n.d	6.72	6.08	5.11	6.48	5.75
Lu_2O_3	n.d	n.d	n.d	n.d	n.d	n.d	n.d	n.d	0.73	0.57	0.61	0.54	1.72
TiO_2	3.37	2.94	1.71	3.05	4.62	3.1	2.14	2.09	1.62	1.53	0.93	0.33	0.67
CaO	0.28	0.28	n.d	n.d	0.07	0.22	0.36	0.45	0.71	0.41	0.97	0.99	0.92
MnO	14.21	14.03	14.95	13.75	14.22	14.15	1.10	1.52	0.61	0.71	0.55	0.53	0.49
Fe_2O_3	6.21	6.61	6.51	6.85	6.12	6.98	18.11	17.25	0.79	0.95	2.85	1.23	0.85
ThO_2	n.d	n.d	n.d	n.d	n.d	n.d	1.75	1.31	2.15	1.14	2.06	2.94	2.33
UO_2	1.07	0.87	n.d	0.71	0.85	1.43	1.24	1.04	3.82	1.22	1.33	0.73	0.71
SiO_2	n.d	n.d	n.d	n.d	n.d	n.d	n.d	n.d	0.69	1.17	1.04	1.49	1.60
Total	99.94	99.8	99.94	99.99	99.98	100.09	100	99.31	99.78	99.95	99.75	100	100
$\sum HREE_2O_3$									18.85	16.91	17.37	16.2	19.08
Cation													
Y	0.03	0.01	0.01	0.01	0.03	0.02	0.00	0.00	0.52	0.53	0.51	0.54	0.55
Nb	1.84	1.86	1.90	1.87	1.80	1.83	1.91	1.93	0.97	1.00	0.99	1.00	0.97
Ta	0.03	0.02	0.03	0.03	0.03	0.03	0.01	0.01	0.01	0.01	0.01	0.01	0.01
Gd									0.02	0.01	0.01	0.01	0.01
Dy									0.05	0.04	0.05	0.03	0.04
Ho									0.01	0.01	0.02	0.01	0.02
Er									0.06	0.06	0.07	0.06	0.07
Tm									0.01	0.02	0.01	0.01	0.03
Yb									0.09	0.08	0.07	0.09	0.08
Lu									0.01	0.01	0.01	0.01	0.02
Ti	0.14	0.12	0.07	0.13	0.19	0.13	0.09	0.09	0.05	0.05	0.03	0.01	0.02
Ca	0.02	0.02	0.00	0.00	0.00	0.01	0.02	0.03	0.03	0.02	0.04	0.05	0.04
Mn	0.68	0.67	0.71	0.65	0.67	0.68	0.05	0.07	0.02	0.03	0.02	0.02	0.02
Fe	0.29	0.31	0.31	0.32	0.29	0.33	0.86	0.82	0.03	0.03	0.09	0.04	0.03
Th	0.00	0.00	0.00	0.00	0.00	0.00	0.02	0.02	0.02	0.01	0.02	0.03	0.02
U	0.01	0.01	0.00	0.01	0.01	0.02	0.02	0.01	0.04	0.01	0.01	0.01	0.01
Si									0.03	0.05	0.04	0.06	0.07
∑Cations	3.03	3.03	3.03	3.02	3.03	3.05	2.99	2.98	1.98	1.96	1.99	1.98	2.00
Ta/(Ta + Nb)	0.01604	0.01064	0.01554	0.01579	0.01639	0.01613	0.00521	0.00515					
Mn/(Mn + Fe)	0.7010	0.6837	0.6961	0.6701	0.6979	0.6733	0.0549	0.0787					

Min., mineral; *oxid.*, oxides

Calculations are based on 6 and 4 oxygen atoms per formula unit (apfu) for columbite and fergusonite, respectively

n.d., not determined

Galena is a lead sulfide mineral and occurs as very fine grains, thin films along the peripheries of sphalerite grains, and/or fine grains along zircon in microgranite (Fig. 9a–d). EPMA data show that Pb concentration reached 85.22 wt% and S 12.73 wt%. Fe and Si are presented as minor constituents, with mean values of 0.51 wt% and 0.89 wt%, respectively.

Sphalerite is a zinc sulfide mineral and occurs as anhedral to subhedral grains and contains thin films of galena along its peripheries in the microgranite (Fig. 9d). EPMA data

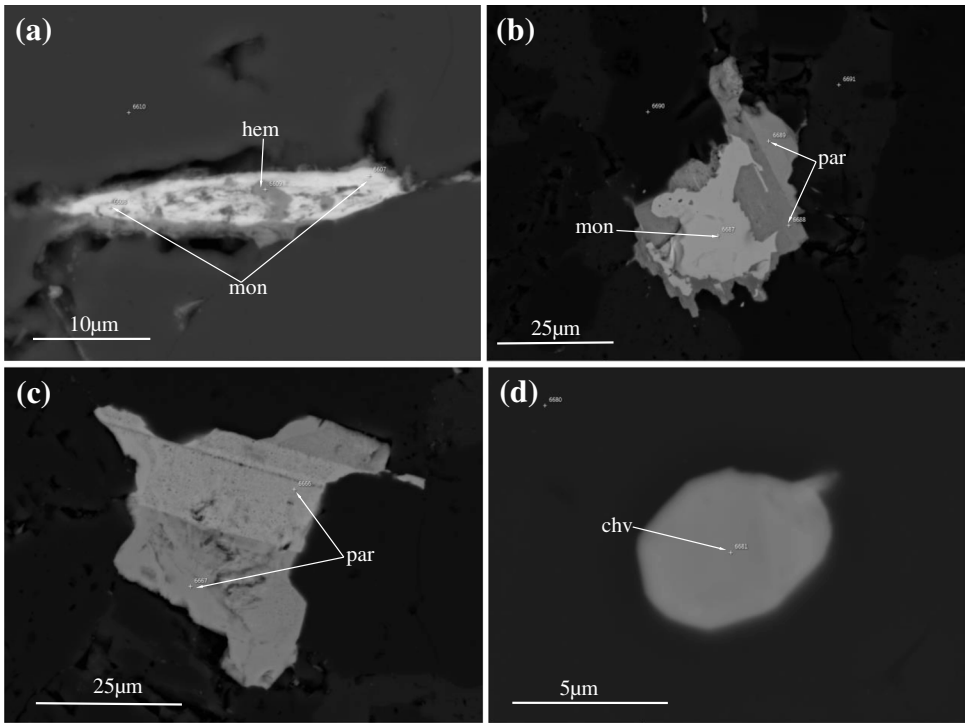

Fig. 8 Back-scattered images of REE-bearing minerals from felsic dikes, Abu Hawis area, North Eastern Desert, Egypt. **a** Micro-veinlet filled with monazite and hematite in microgranite; **b** corroded parisite crystal enclosing monazite in rhyolite; **c** anhedral crystal of parasite in rhyolite; **d** fine-grained chevkinite in rhyolite. Abbreviations: mon, monazite; par, parisite; chv, chevkinite; hem, hematite

show that sphalerite is composed mainly of Zn reaching 61.59 wt% and S 34.91 wt%. Si and Fe occurred as minor constituents, reaching 0.69 and 2.22 wt%, respectively. Fluorite occurs as anhedral to subhedral grains in the rhyolite. It occurs also as fine-grained and is associated with thorite, parisite, and hematite (Fig. 5c). EPMA data show that fluorite is composed mainly of Ca 52.23 wt% and F 45.72 wt%, with minor amounts of Si 0.19 wt%.

Apatite occurs as anhedral grains in the rhyolite and is associated with parisite and thorite (Fig. 5d). EPMA data show that the main constituents of apatite are CaO 55.03 wt% and P_2O_5 42.07 wt%. SiO_2 occurs as minor constituent 0.41 wt% whereas F reached to 5.34 wt% designating fluorapatite.

Discussion

The E–W and NE–SW control of rare metal mineralization

Felsite dike swarms are almost abundant and numerous in the North Eastern Desert of Egypt, having E–W and NE–SW (Ali 2007, Dessouky et al. 2020; Waheeb and EL Sundoly 2020). The distribution of felsite dikes confirms that a gradual transition from N-S extension trend to NE–SW and NW–SE extension trends was occurred in Abu Hawis area (Ali 2007; Waheeb and EL Sundoly 2020).

Ali (2009) states that a marked positive correlation was taken place between the extensional events and the NE–SW, NW–SE, and E–W trends. These events led to U-migration from Abu Hawis monzogranite to be deposited along the main shear zones trending in the NE–SW direction. These trends dominate on the mobility map (eU-eTh/3.5), and show NW–SE, NE–SW, and N–S extensional trends, respectively.

Abu Hawis granitoids are located to the northeast of El-Erediya granites enriched in U mineralization especially in jasper veins having NE–SW to ENE–WSW-striking fractures that dated 130–160 Ma for hydrothermal event (Abu-Deif 1992). Besides, the studied area is located in the western part of Ras Abda syenogranite. Age dating of the magmatic crystallization for Ras Abda mineralized syenogranite is 610 Ma (Dessouky et al. 2020; Abdel Gawad et al. 2021a, b, c), whereas the age of the hydrothermal event is 126.8 ± 2.0 Ma (Abdel Gawad et al. 2021a, b, c). These trends could have been reactivated many times at different ages. Therefore, they may be used as good indicators for the existence U mineralization that is associated with other rare metal mineralization.

Post-magmatic and hydrothermal processes controlling mineralization

The radioactive mineralizations — including uraninite, thorite, and uranothorite — are well recorded in felsic dikes. They could be of a syn-genetic origin during their emplacement along E–W and NE–SW structural trends. The sulfide

Table 4 Representative EPMA data (oxides, in wt%) of monazite from the studied felsic dikes, Abu Hawis area, North Eastern Desert, Egypt

Min. in dike/oxid	Monazite in microgranite					Aver	Monazite in rhyolite				Aver
SiO_2	0.19	0.26	0.29	0.28	0.25	0.25	0.24	0.22	0.23	0.19	0.22
CaO	0.43	0.41	0.24	0.22	0.22	0.30	0.29	0.32	0.28	0.34	0.31
P_2O_5	26.66	29.18	30.91	30.98	29.02	29.35	29.32	28.48	29.31	29.21	29.08
Fe_2O_3	0.24	0.28	0.31	0.25	0.19	0.25	0.31	0.37	0.29	0.42	0.35
La_2O_3	9.23	9.86	10.25	8.69	7.81	9.17	16.12	15.88	16.14	15.25	15.85
Ce_2O_3	31.79	29.5	28.76	31.95	30.12	30.42	32.24	32.42	32.74	33.06	32.62
Pr_2O_3	4.27	4.58	3.99	4.19	4.73	4.35	3.44	2.67	2.87	3.48	3.12
Nd_2O_3	11.14	12.52	9.93	10.17	12.19	11.19	14.03	13.95	14.12	14.56	14.17
Sm_2O_3	2.39	2.11	1.95	1.60	2.18	2.05	1.83	2.16	1.19	1.23	1.60
Gd_2O_3	1.37	1.18	1.09	1.16	1.20	1.20	0.63	0.74	0.87	0.92	0.79
ThO_2	11.96	10.11	11.98	10.51	11.87	11.29	1.55	2.16	1.19	1.23	1.53
Total	99.67	99.99	99.7	100	99.78	99.83	100	99.37	99.23	99.89	99.62
$\sum REE_2O_3$	60.19	59.75	55.97	57.76	58.23	58.38	68.29	67.82	67.93	68.5	68.14
Cation	Calculated chemical formulae are based on 4 oxygen atoms (apfu)										
Si	0.01	0.01	0.01	0.01	0.01	0.01	0.01	0.01	0.01	0.01	0.01
Ca	0.02	0.02	0.01	0.01	0.01	0.01	0.01	0.01	0.01	0.01	0.01
P	0.94	0.99	1.02	1.02	0.99	0.99	0.98	0.97	0.99	0.98	0.98
Fe	0.01	0.01	0.01	0.01	0.01	0.01	0.01	0.01	0.01	0.01	0.01
La	0.14	0.15	0.15	0.12	0.12	0.14	0.24	0.24	0.24	0.22	0.23
Ce	0.49	0.43	0.41	0.45	0.44	0.44	0.47	0.48	0.48	0.48	0.47
Pr	0.06	0.07	0.06	0.06	0.07	0.06	0.05	0.04	0.04	0.05	0.05
Nd	0.17	0.18	0.14	0.14	0.18	0.16	0.20	0.20	0.20	0.21	0.20
Sm	0.03	0.03	0.03	0.02	0.03	0.03	0.02	0.03	0.02	0.02	0.02
Gd	0.02	0.02	0.01	0.01	0.02	0.02	0.01	0.01	0.01	0.01	0.01
Th	0.11	0.09	0.11	0.09	0.11	0.10	0.01	0.02	0.01	0.01	0.01
∑cations	2.00	1.98	1.95	1.96	1.97	1.97	2.01	2.02	2.01	2.01	2.01

Min., mineral; *oxid.*, oxides; *Aver.*, average

$\sum REE_2O_3$ ($La_2O_3 + Ce_2O_3 + Pr_2O_3 + Nd_2O_3 + Sm_2O_3 + Gd_2O_3$)

n.d., not determined

minerals in the microgranite are pyrite, sphalerite, and galena as accessories associated with U and Th minerals.

The total analyses of thorite from both microgranite and rhyolite are often close to 90 wt% (Table 1) due to strong hydration or metamictization (Abd El-Naby 2009; Gaafar et al. 2014; Abdel Gawad 2021). Some grains of thorite are enclosed in hematite, in which could be a good indicator of strong alteration.

Zircon crystals incorporate micro-inclusions of uraninite, thorite, uranothorite, monazite, and zircon into their crystal lattice, which could enhance metamictization of zircon (Alekseev and Alekseev 2020; Levashova et al. 2021) (Fig. 4a). The presence of fine-grained zircon as inclusions in large zircon crystals indicates the occurrence of two zircon generations in the studied microgranite dikes. EPMA data show higher HfO_2 that reached 9.08 wt% in the analyzed zircon crystals from microgranite dikes. This could be a good indicator for the hydrothermal activities, according to Wang et al. (2010).

The calculated Ta/(Ta + Nb) and Mn/(Mn + Fe) ratios of the analyzed columbite from microgranite range between (0.0052 and 0.0164) and (0.0549 and 0.7010), respectively, which indicate manganocolumbite composition. Fergusonite is the most dominated HREE-bearing mineral recorded in the microgranite with a mean ΣHRE_2O_3 17.68 wt%. On the other hand, parisite and chevkinite are LREE minerals recorded in the rhyolite with means ΣLRE_2O_3 53.53 and 43.75 wt%. However, monazite is a dominated LREE mineral in both microgranite and rhyolite with means ΣLRE_2O_3 58.38 and 68.14 wt%.

High field strength elements (HFSE) Zr, Hf, Th, and Ti are generally mobile elements during magmatic stage, and/or hydrothermal alterations containing complexing agents as F, S, and others (Keppler 1993; Ali 2012). Abu Hawis, Umm Tagher El Foqani, and Ras Barud monzogranites are enriched in HFSE (Zr, Hf, Th, and Ti), as well as rare metal mineralization. It is well known that F could have a prominent role during mobilization of Zr, Hf, Th, and Ti as well

Table 5 Representative EPMA data (oxides, in wt%) of parisite and chevkinite from rhyolite, Abu Hawis area, North Eastern Desert, Egypt

Min/oxid	Parisite								Aver	Chevkinite	
SiO_2	0.13	0.16	0.11	0.13	0.08	0.12	0.13	0.09	0.12	19.79	19.97
CaO	13.8	14.87	14.08	13.89	12.84	13.75	13.55	13.64	13.80	1.21	1.65
P_2O_5	n.d	n.d	n.d	n.d	n.d	n.d	n.d	n.d	n.d	0.09	n.d
TiO_2	n.d	n.d	n.d	n.d	n.d	n.d	n.d	n.d	n.d	20.35	19.25
Fe_2O_3	n.d	n.d	n.d	n.d	n.d	n.d	n.d	n.d	n.d	13.11	12.59
La_2O_3	14.58	13.64	14.05	13.9	14.72	14.21	13.62	13.27	14.00	11.38	11.56
Ce_2O_3	22.72	22.73	23.91	22.64	23.77	22.18	22.09	23.9	22.99	21.52	21.85
Pr_2O_3	3.08	3.17	3.03	2.89	3.01	2.94	3.06	2.98	3.02	1.78	1.85
Nd_2O_3	10.74	10.92	12.24	11.35	11.55	12.48	12.26	12.12	11.71	7.87	8.24
Sm_2O_3	1.41	1.48	1.61	1.61	1.31	1.42	1.53	1.54	1.49	0.73	0.71
Gd_2O_3	0.32	0.34	0.37	0.31	0.30	0.26	0.35	0.29	0.32	n.d	n.d
ThO_2	0.49	0.62	0.79	0.45	0.44	0.90	0.75	0.65	0.64	1.98	2.11
UO_2	n.d	n.d	n.d	n.d	n.d	n.d	n.d	n.d	n.d	0.18	0.22
F	8.56	7.81	8.45	8.72	8.69	8.73	8.19	8.09	8.41	n.d	n.d
Total	75.83	75.74	78.64	75.89	76.71	76.99	75.53	76.57	76.49	99.99	100
$\sum REE_2O_3$	52.85	52.28	55.21	52.7	54.66	53.49	52.91	54.1	53.53	43.28	44.21
Cation											
Si	0.01	0.01	0.01	0.01	0.01	0.01	0.01	0.01	0.01	4.03	4.10
Ca	1.03	1.11	1.02	1.03	0.95	1.01	1.02	1.02	1.02	0.26	0.36
P										0.02	0.00
Ti										3.12	2.98
Fe										2.23	2.16
La	0.37	0.35	0.35	0.35	0.38	0.36	0.35	0.34	0.36	0.86	0.88
Ce	0.58	0.58	0.59	0.57	0.60	0.56	0.57	0.61	0.58	1.68	1.72
Pr	0.08	0.08	0.07	0.07	0.08	0.07	0.08	0.08	0.08	0.14	0.15
Nd	0.27	0.27	0.30	0.28	0.29	0.31	0.31	0.30	0.29	0.57	0.60
Sm	0.03	0.04	0.04	0.04	0.03	0.03	0.04	0.04	0.04	0.05	0.05
Gd	0.01	0.01	0.01	0.01	0.01	0.01	0.01	0.01	0.01		
Th	0.01	0.01	0.01	0.01	0.01	0.01	0.01	0.01	0.01	0.09	0.10
U										0.01	0.01
F	1.88	1.72	1.81	1.90	1.90	1.89	1.82	1.78	1.84		
∑cations	4.25	4.18	4.20	4.27	4.25	4.26	4.21	4.19	4.23	13.07	13.11

Min., mineral; *oxid.*, oxides; *Aver.*, average

Calculated formulae (apfu) of parasite are based on number of ions on the basis of two fluorine apfu on the basis of $(CO_3)_3F_2$

Chevkinite formulae is calculated on the basis of 22 oxygen per formula unit (apfu)

n.d., not determined

as REE (Moine and Salvi 1999) during hydrothermal alterations (argillic and hematitization).

The reactivated structures are accompanied in association with succession fluid circulations leading to the injection of a series of microgranite, rhyolite, andesite, and basaltic dikes as well as quartz veins. Changes in host rock composition and mineralogy are used to decipher the type and extent of fluid–wall rock interactions during alteration. The physico–chemical conditions of these fluids were changing due to consequent reactions with the granitoids and post-granitic dikes with meteoric water.

The hydrolysis of K-feldspar and plagioclase into illite or Na-montmorillonite (K-alteration) according to the reactions (1, 2, and 3) (Pirajno 1992).

$$3KAlSi_3O_{8\ \text{K-feldspar}} + 2H^+_{\text{acidicfluids}} \rightarrow KAl_2(Si_3AlO_{10})(OH)_{2\ \text{illite}} + 2K^+ + 6SiO_{2\ \text{quartz}} \quad (1)$$

$$6NaAlSi_3O_{8\ \text{Na-plagioclase}} + 2K^+ + 4H^+ \rightarrow 2KAl_2(Si_3AlO_{10})(OH)_{2\ \text{illite}} + 12SiO_{2\ \text{quartz}} + 6Na^+ \quad (2)$$

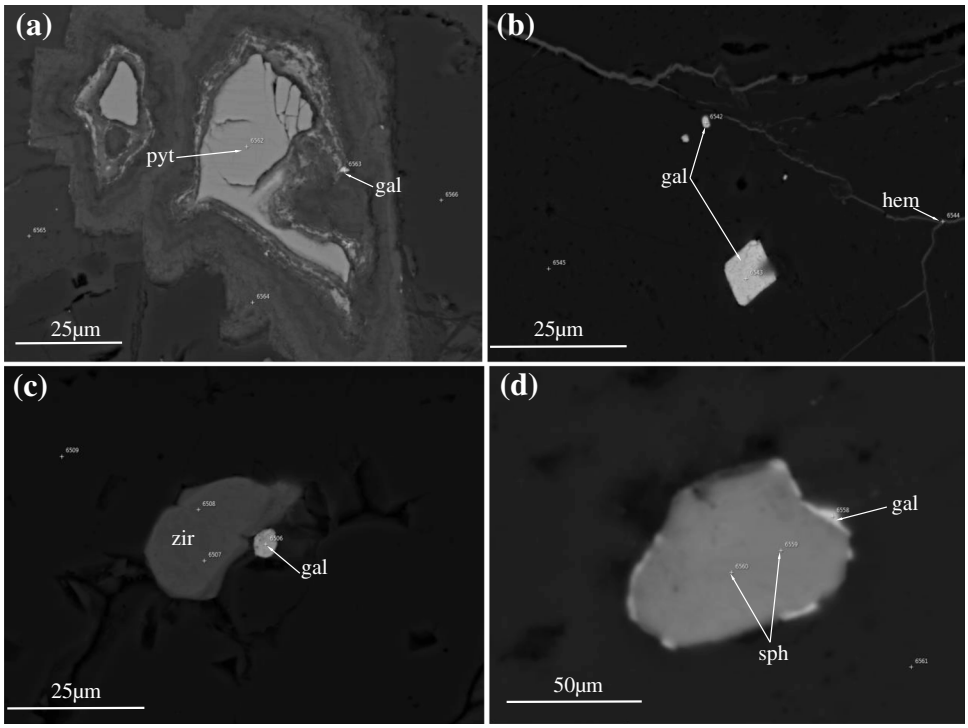

Fig. 9 Back-scattered images of sulfide minerals from microgranite, Abu Hawis area, North Eastern Desert, Egypt. **a** Pyrite associated with very fine grains of galena, enclosed in plagioclase; **b** fine grains of galena, associated with micro-veinlets of hematite, enclosed in K-feldspar; **c** fine grain of galena occurs along the peripheries of zircon crystal; **d** thin film of galena occurring along the peripheries of sphalerite grain. Abbreviations: zir, zircon; pyt, pyrite; gal, galena; sph, sphalerite; hem, hematite

$$1.17NaAlSi_3O_{8\ \mathrm{Na-plagioclase}} + H^+ \rightarrow 0.5Na_{0.33}Al_{2.33}Si_{3.67}O_{10}(OH)_{2\ \mathrm{Na-montmorillonite}} + 1.67SiO_{2\ \mathrm{quartz}} + Na^+ \quad (3)$$

The hydrolysis of illite and Na-montmorillonite produces kaolinite according to the following reactions (4 and 5), respectively (Pirajno 1992).

$$KAl_2(Si_3AlO_{10})(OH)_{2\ \mathrm{illite}} + H^+ + 1.5H_2O \rightarrow 1.5Al_2Si_2O_5(OH)_{4\ \mathrm{kaolinite}} + K^+ \quad (4)$$

$$3Na_{0.33}Al_{2.33}Si_{3.67}O_{10}(OH)_{2\ \mathrm{Na-montmorillonite}} + H^+ + 3.5H_2O \rightarrow 3.5Al_2Si_2O_5(OH)_{4\ \mathrm{kaolinite}} + 4SiO_{2\ \mathrm{quartz}} + Na^+ \quad (5)$$

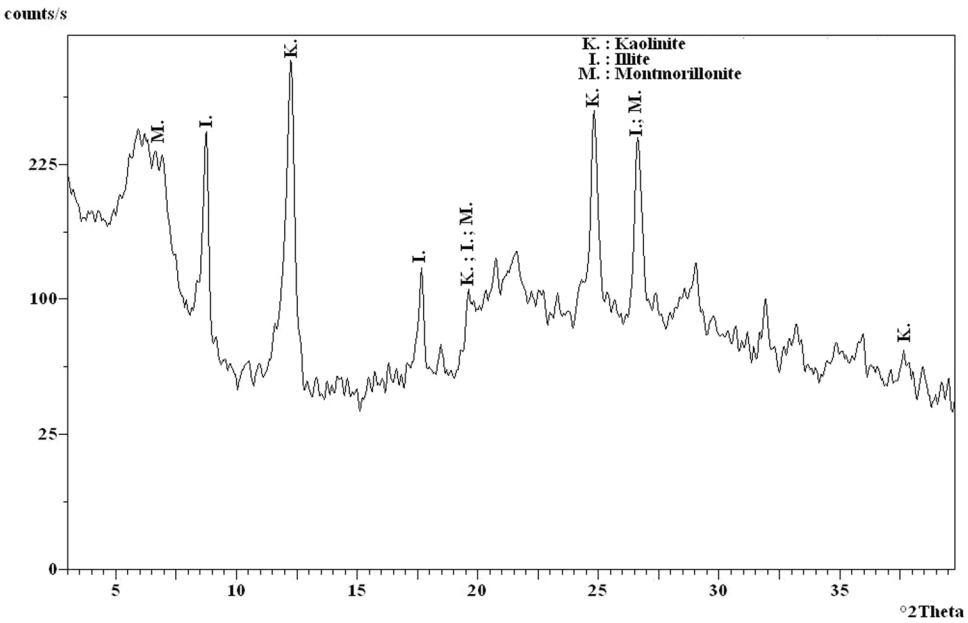

Fig. 10 XRD for clay alteration products (montmorillonite, illite, and kaolinite), Abu Hawis area, North Eastern Desert, Egypt

Table 6 X-ray diffraction data of clay alteration products, Abu Hawis area, North Eastern Desert, Egypt

Clay alteration products		Identified minerals					
		Montmorillonite		Illite		Kaolinite	
		ASTM card no					
		13–0135		9–0343		06–221	
dÅ	I/I_0	dÅ	I/I_0	dÅ	I/I_0	dÅ	I/I_0
15	99	15	100				
10.10	100			10	100		
7.20	72					7.18	100
5.02	26			4.95	80		
4.52	8	4.5	80	4.48	90	4.48	80
3.58	15					3.58	100
2.5	2	2.5	40	2.5	10		
2.39	1					2.386	80

Clay alteration products have been identified by using XRD analyses (Fig. 10 and Table 6).

Monazite, parisite, and chevkinite are associated with fluorapatite in the rhyolite dikes. These LREE minerals are poor in Th (Tables 4 and 5), with the absence of U and/or the presence with minor concentrations in chevkinite (up to 0.22 wt%). In this case of LREE minerals, the compositional features could suggest their formation as a result of fluorapatite metasomatism (Ziemann et al. 2005; Ali 2012). On the other hand, the chemical composition of monazite from the microgranite shows high Th contents, with a mean of ThO_2 11.29 wt%, which could indicate magmatic monazite.

Conclusions

1- The investigated felsic dikes having E–W and NE–SW trends at Abu Hawis area show a marked enrichment of rare metal mineralization, through the use of electron probe microanalysis.
2- Uraninite, uranothorite, and thorite are recorded in the microgranite dikes, while the latter one is only recorded in the rhyolite dikes. UO_2 contents reached up to 69.57, 27.42, and 5.33 wt% in the analyzed uraninite, uranothorite, and thorite from the microgranite dikes. HREEs (Dy_2O_3, Er_2O_3, and Yb_2O_3) were recorded as minor amounts in uraninite and thorite, but absent in uranothorite.
3- Both ThO_2 and UO_2 show low concentrations in zircon crystals, whereas HfO_2 shows high values up to 9.08 wt% from the microgranite dikes. This could be related to strong hydrothermal alteration (hematitization). HREE and Y_2O_3 are well presented in zircon crystals from the rhyolite dikes.
4- Nb-bearing minerals are well represented by columbite and fergusonite from the microgranite dikes. Columbite is enriched in manganese relative to iron and this could indicate the formation of manganocolumbite composition, except in only two analyses that are ferrocolumbite composition. Fergusonite is enriched in Nb_2O_5, Y_2O_3, and $HREE_2O_3$ that reached up to 51.95, 23.64, and 19.08 wt%.
5- REE minerals including monazite are well predominated in both the microgranite and the rhyolite dikes, with mean values of P_2O_5 (29.35 to 29.08 wt%), ThO_2 (11.29 to 1.53 wt%), and $LREE_2O_3$ (58.38 to 68.14 wt%). Parisite and chevkinite are recorded only in the rhyolite dikes. They are enriched in LREE, where Ce_2O_3 is the most predominant REE that reaches up to 21.85–23.91 wt%, followed by La_2O_3 11.56–14.00 wt%, then Nd_2O_3 8.24–11.71 wt%, with minor amounts of other element in both parisite and chevkinite, respectively.

Acknowledgements I wish to expresses my deepest gratitude and acknowledgments to Prof. Elena Panova, Dr. Mohamed Ghoneim, and Prof. Svetlana Yanson for providing EPMA analyses at the Geomodel Research Center, St. Petersburg State University, Russia. The author is grateful to Prof. Ahmed A. Ammar, Prof. Masoud Salah, and Prof. Sayed Omar, Nuclear Materials Authority of Egypt for their fruitful discussion and help during this work. I would like to thank the Associate Editor Prof. Federico Lucci and the anonymous reviewer for their constructive and valuable comments that have helped to improve the manuscript.

Funding Open access funding provided by The Science, Technology & Innovation Funding Authority (STDF) in cooperation with The Egyptian Knowledge Bank (EKB).

Declarations

Conflict of interest The author declares that he has no competing interests.

References

Abd El-Naby HH (2009) High and low temperature alteration of uranium and thorium minerals, Um Ara granites, south Eastern Desert, Egypt. Ore Geol Rev 35:436–446

Abdalla HM, Helba H, Mohamed FH (1998) Chemistry of columbite-tantalite minerals in rare metal granitoids, Eastern Desert, Egypt. Mineral Mag 62:821–836

Abdel Gawad AE (2021) Mineral chemistry (U, Th, Zr, REE) in accessory minerals from Wadi Rod Elsayalla granitoids, South Eastern Desert, Egypt. Arab J Geosci 14(1996):1–17. https://doi.org/10.1007/s12517-021-08367-7

Abdel Karim MA, Sos EA (2000) Geochemical characteristics and potassium argon ages dating of some granitoids from South Eastern Desert, Egypt. Eg J Geol Soc Egypt 44:305–318

Abdel Wahed AA, Ali KG, Khalil MM, Abdel Gawad AE (2012) Dokhan volcanics of Gabal Moqul area, North Eastern Desert, Egypt: geochemistry and petrogenesis. Arab J Geosci 5:29–44. https://doi.org/10.1007/s12517-010-0136-z

Abdel Gawad AE, Skublov SG, Levashova EV, Ghoneim MM (2021a) Geochemistry and U–Pb age dating of zircon as a petrogenetic tool for magmatic and hydrothermal processes in Wadi Ras Abda syenogranite, Eastern Desert, Egypt. Arab J Geosci Eng 1–15, https://doi.org/10.1007/s13369-021-06319-7

Abdel Gawad AE, Ghoneim MM, El-Taher A, Ramadan AA (2021b) Mineral chemistry aspects of U-, Th-, REE-, Cu-bearing minerals at El-Regeita shear zone, South Central Sinai. Egypt Arab J Geosci 14:1–13. https://doi.org/10.1007/s12517-021-07801-0

Abdel Gawad AE, Ali MA, Ghoneim MM, El-Taher A (2021c) Natural radioactivity and mineral chemistry aspects of rare metal mineralisation associated with mylonite at Wadi Sikait, South Eastern Desert, Egypt. Int J Environ Anal Chem 1–18, https://doi.org/10.1080/03067319.2021.1891416

Abdel Gawad AE, EneSkublov ASG, Gavrilchik AK, Ali MA, Ghoneim MM, Nastavkin AV (2022) Trace element geochemistry and genesis of beryl from Wadi Nugrus, South Eastern Desert, Egypt. Minerals 12:206. https://doi.org/10.3390/min12020206

Abdellah WM, Khalafalla MS, Abu Khoziem HA, El Hussaini OM (2021) Physical and chemical processes of Abu Rusheid cataclastic rocks for recovering niobium, zirconium and uranium compounds. Physicochem Probl Miner Process 57(5):137–154

Abu Dief A (1992) The relation between uranium mineralization and tectonics in some Pan-African granites, West of Safaga, Egypt. Unpublished Ph.D. Thesis. Assiut Univ Assiut, Egypt, 218 p

Ahmed FY, Moharem AF (2002) Genesis of uranium in the younger granites of Gabal Abu Hawis area, Central Eastern Desert, Egypt. Sixth Arab Conference on the Peaceful of Atomic Enemy, Cairo, Egypt, 14–19 Dec. EGO400152

Al-Boghdady AA, Omar SA, Bayoumi MM (2005) Geological and petrological investigations on Gabal Abu Hawis area, Central Eastern Desert, Egypt. The 4th Intern. Conf Geol of Africa Assiut Univ November 15-16, Assiut, Egypt, 1, 267–287

Alekseev VI, Alekseev IV (2020) Zircon as a mineral indicating the stage of granitoid magmatism at Northern Chukotka, Russia. Geosci 10:194. https://doi.org/10.3390/geosciences10050194

Ali BH (2015) SHRIMP U-Pb zircon geochronology: evidence for emplacement time of some granitoids north Eastern Desert, Egypt Arab. J Geosci 8:5465–5474. https://doi.org/10.1007/s12517-014-1608-3

Ali KG (2007) Structural controls of uranium anomalies in the Abu Hawis shear zone, Central Eastern Desert, Egypt. Irish Assoc Econ Geol 1181–1184. http://119.78.100.177/qdio/handle/2XILL650/296460

Ali MA (2012) Mineral chemistry of monazite-(Nd), xenotime-(Y), apatite, fluorite and zircon hosting in lamprophyre dyke in Abu Rusheid area, South Eastern Desert, Egypt. Geologija, 55/1, 93–106, Ljubljana; https://doi.org/10.5474/geologija.2012.007

Ali MA, Abdel Gawad AE, Ghoneim MM (2021) Geology and mineral chemistry of uranium and thorium bearing minerals in rare-metal (NYF) pegmatites of Um Solimate, South Eastern Desert of Egypt. Acta Geolo Sin (english Edition) 95(5):1568–1582. https://doi.org/10.1111/1755-6724.14708

Ammar SE, Omar SA, Baghdady AA, Gaafar IM, Bayoumi MM (2007) Ground gamma ray spectrometric patterns in Abu Hawis granites, Central Eastern Desert, Egypt. 2nd Int Conf Geol Tethys Cairo Univ March 2007, 521–533

Bagiński B, Macdonald R, Dzierżanowski P, Zozulya D, Kartashov PM (2015) Hydrothermal alteration of chevkinite-group minerals: products and mechanisms. Part 1. Hydration of chevkinite-(Ce). Mineral Mag 79:1019–1037

Bourzac K (2001) The rare-earth crisis. Tech Rev Manch 114(3):58–63

Černý P, Ecrit TS (1985) Some recent advances in the mineralogy and geochemistry of Nband Ta in rare-element granitic pegmatites. Bull De Mineralogie 108:499–532

Dawoud M, Abdel Ghani IM, Elsaid M, Badr YS (2017) The integration of ASTER imagery and airborne gamma-ray spectrometry in lithological discrimination of Ras Barud-Um Tagher Area, North Eastern Desert, Egypt. IJISET - Int J Innov Sci Eng Technol 2348–7968

Dawoud MI, Saleh GM, Shahin HA, Khaleal FM, Emad BM (2018) Younger granites and associated pegmatites of Gabal El Fereyid-Wadi Rahaba area, south Eastern Desert, Egypt: geological and geochemical characteristics. Geosci Res 3:29–50

Dessouky OK, Sun W, Ibrahim WS, Ali HH, Hassan MM, Li C, Omran AA, Dardier AM (2020) New insights into Cryogenian arc granitoids hosting Th-U mineralized Ediacaran syenogranite dikes Ra's Abdah Area in the Northern Egyptian Nubian Shield: constraints from U-Pb Ages and Zircon Geochemistry. Precam Res. https://doi.org/10.1016/j.precamres.2020.105986

Eggert R, Wadia C, Anderson CG, Bauer D, Fields F, Meinert LD, Patrick R (2010) Taylor PR (2010) Rare earths: market disruption, innovation and global supply chains. Ann Rev Envir Res 41(1):15–26

El-Bialy MZ, Omar MM (2015) Spatial association of Neoproterozoic continental arc I-type and post-collision A-type granitoids in the Arabian-Nubian Shield: the Wadi Al-Baroud Older and Younger Granites, North Eastern Desert, Egypt. J Afr Earth Sci 103:1–29

Eliwa HA, Breitkreuz C, Murata M, Khalaf IM, Bühler B, Itaya T, Takahashi T, Hirahara Y, Miyazaki T, Kimura J-I, Shibata T, Koshi Y, Kato Y, Ozawa H, Daas MA, El Gameel Kh (2014) SIMS zircon U-Pb and mica K–Ar geochronology, and Sr–Nd isotope geochemistry of Neoproterozoic granitoids and their bearing on the evolution of the north Eastern Desert, Egypt. Gondwana Res 25:1570–1598

Farahat ES, Zaki R, Hauzenberger C, Sami M (2011) Neoproterozoic calc-alkaline peraluminous granitoids of the Deleihimmi pluton, Central Eastern Desert, Egypt: implications for transition from late- to post-collisional tectonomagmatic evolution in the northern Arabian-Nubian Shield. Geol J 46:544–560

Fathy D, Wagreich M, Zaki R, Mohamed RSA, Gier S (2018) Geochemical fingerprinting of Maastrichtian oil shales from the Central Eastern Desert, Egypt: implications for provenance, tectonic setting, and source area weathering. Geol J 53:2597–2612

Fawzy MF, Mahdy NM, Sami M (2020) Mineralogical characterization and physical upgrading of radioactive and rare metal minerals from Wadi Al-Baroud granitic pegmatite at the Central Eastern Desert of Egypt. Arab J Geosci 13:413. https://doi.org/10.1007/s12517-020-05381-z

Gaafar I, Cuney M, Abdel Gawad AE (2014) Mineral chemistry of two-mica granite rare metals: impact of geophysics on the distribution of uranium mineralization at El Sela shear zone. Egypt Open J Geol 4:137–160. https://doi.org/10.4236/ojg.2014.44011

Gambogi J (2013) Rare Earths; USGS Minerals Yearbook–2011; U.S. Department of the Interior, U.S. Geological Survey: Washington, DC, 2013; 60.1–60

German CR, Elderfield H (1990) Application of the Ce anomaly as a paleoredox indicator: the ground rules. Paleoceanography 5:823–833

Ghoneim MM, Panova EG, Abdel Gawad AE (2021) Natural radioactivity and geochemical aspects of radioactive mineralisation in El Sela, South Eastern Desert, Egypt. Int J Environ Anal Chem 1–22. https://doi.org/10.1080/03067319.2021.1892665

Ghoneim MM, Panova EG, Abdel Gawad AE, Yanson SY (2020) Morphology and geochemical features of zircon from intrusive rocks of El Sela area, Eastern Desert, Egypt. News Ural State Min Univ 3(59):C. 7-18. https://doi.org/10.21440/2307-2091-2020-3-7-18

Heikal MThS, Khedr MZ, Abd El Monsef M, Gomaa SR (2019) Petrogenesis and geodynamic evolution of Neoproterozoic Abu dabbab albite granite, Central Eastern Desert of Egypt: petrological and geochemical constraints. J Afr Earth Sci 158:103518

Heikal MThS, Moharem AF, El Nashar ER (2001) Petrogenesis and radioactive inspection of Li mica pegmatites at Wadi Zareib, central Eastern Desert, Egypt. 2nd Int Conf Conf Geol Africa Assiut, II: 227–305

Hoatson DM, Jaireth S and Miezitis Y (2011) The major rare-earth element deposits of Australia: geological setting, exploration, and resources. Geosci Aust 204 p

Jaireth S, Hoatson DM, Miezitis Y (2014) Geological setting and resources of the major rare-earth-element deposits of Australia. Ore Geol Rev 62:72–128

Johnson PR, Woldehaimanot B (2003) Development of the Arabian-Nubian shield: perspectives on accretion and deformation in the Northern East African orogen and the assembly of Gondwana. Spec Publ Geol Soc Lond 206:289–325

Keppler H (1993) Influence of fluorite on the enrichment of high field strength trace elements in granitic rocks. Contrib Mineral Petrol 114:479–788

Levashova EV, Skublov SG, Popov VA (2021) Distribution of trace elements controlled by sector and growth zonings in zircon from feldspathic pegmatites (Ilmen Mountains, the Southern Urals). Geosci 11:7. https://doi.org/10.3390/geosciences11010007

Liégeois JP, Stern RJ (2010) Sr-Nd isotopes and geochemistry of granite-gneiss complexes from the Meatiq and Hafafit domes, Eastern Desert, Egypt: no evidence for pre-Neoproterozoic crust. J Afr Earth Sci 57:31–40

Linnen RL, Van Lichtervelde M, Černý P (2012) Granitic pegmatites as sources of strategic metals. Elements 8:275–280. https://doi.org/10.2113/gselements.8.4.275

Liu X, Wang Q, Feng Y, Li Z, Cai S (2013) Genesis of the Guangou karstic bauxite deposit in western Henan, China. Ore Geol Rev 55:162–185

Macdonald R, Bagiński B, Kartashov P, Zozulya D, Dzierżanowski P (2012) Chevkinite-group minerals from Russia and Mongolia: new compositional data from fenites, metasomatites and ore deposits. Mineral Mag 76:535–549

Mahdy NM (2021) Textural and chemical characteristics of zircon, monazite, and thorite, Wadi Al-Baroud area, Eastern Desert of Egypt: implication for rare metal pegmatite genesis. Ore Geol Rev 136:104225. https://doi.org/10.1016/j.oregeorev.2021.104225

Mariano AN, Mariano A Jr (2012) Rare earth mining and exploration in North America. Elements 8:369–376

Moine B, Salvi S (1999) Role of fluorine-rich fluids in the hydrothermal transport of "immobile" elements (Th, Zr, REE). Bull Deliaison de la Societe Francaise de Mineralogie et de Cristallographie (S. F. M. C.) 11: 90–92

Moussa EMM, Stern RJ, Manton WI, Ali KA (2008) SHRIMP zircon dating and Sm/Nd isotopic investigations of Neoproterozoic granitoids, Eastern Desert, Egypt. Precam Res 160:341–356

Pirajno F (1992) Hydrothermal mineral deposits—principles and fundamental concepts for the exploration geologist. Springer, Berlin

Raslan MF, El-Shall HE, Omar SA, Daher AM (2010) Mineralogy of polymetallic mineralized pegmatite of Ras Baroud granite, Central Eastern Desert, Egypt. J Mineral Petrol Sci 105:123–134

Saleh GM (2007) Rare-metal pegmatites from the Southeastern Desert, Egypt: geology, geochemistry, and petrogenesis. Int Geol Rev 49(9):824–843

Skublov SG, Abdel Gawad AE, Levashova EV, Ghoneim MM (2021) U-Pb geochronology, REE and trace element geochemistry of zircon from El Fereyid monzogranite, south Eastern Desert, Egypt. J Mineral Petrol Sci 116(4):220–233

Surour AA (2021) Sn-W-Ta-Mo-U-REE mineralizations associated with alkali granite magmatism in Egyptian Nubian Shield. In: Hamimi Z, Arai S, Fowler A, El-Bialy MZ (eds) The geology of the Egyptian Nubian Shield, regional geology reviews, Springer Nature Switzerland, 593–604. https://doi.org/10.1007/978-3-030-49771-2

Surour AA, Omar SAM (2020) Historiography and FTIR spectral signatures of beryl crystals from some ancient Roman sites in the Eastern Desert of Egypt. Environ Earth Sci 79(520):1–15. https://doi.org/10.1007/s12665-020-09260-4

Surour AA, Omar SMA (2022) Chemical and spectroscopic characterization of tourmaline from the ancient Roman mines in the Eastern Desert of Egypt. Environ Earth Sci 81:78. https://doi.org/10.1007/s12665-022-10215-0

Waheeb AG, El Sundoly HI (2020) Tensile stress and related Th-U-REE mineralizations in the granite of Wadi Ras Abda, North Eastern Desert, Egypt. Arab J Geosci 13:659. https://doi.org/10.1007/s12517-020-05543-z

Wang X, Griffin WL, Chen J (2010) Hf contents and Zr/Hf ratios in granitic zircons. Geochem J 44:65–72

Zepf V (2013) Rare earth elements: what and where they are. In Rare earth elements: a new approach to the nexus of supply, demand, and use: exemplified along the use of neodymium in permanent magnets. Zepf V (Ed) Springer Theses; Springer-Verlag, Berlin-Heidelberg, Germany, 11–39

Ziemann MA, Förster HJ, Harlov DE, Frei D (2005) Origin of fluorapatite–monazite assemblages in a metamorphosed, sillimanite bearing pegmatoid, Reinbolt Hills, East Antarctica. Eur J Mineral 17:567–579